

# Simultaneous Real-Time Estimation of Atmospheric Density and Ballistic Coefficient\*

James R. Wright    James Woodburn  
Analytical Graphics, Inc.

February 1, 2004

## Abstract

Atmospheric drag is a significant force for all spacecraft in LEO. Given the appropriate use of current best geopotential functions for gravity modeling, the most significant LEO estimation errors are due to atmospheric drag modeling. Historically, a ballistic coefficient estimate has been used to absorb atmospheric density modeling errors, as well as ballistic coefficient modeling errors. *The purpose herein is to demonstrate the simultaneous real-time estimation of both atmospheric density and ballistic coefficient* with simulated range data and with real range data. The approach tested is valid when the exponential half-life on ballistic coefficient errors is significantly different than that on atmospheric density errors. Though correlated, atmospheric density modeling errors and ballistic coefficient modeling errors are shown to be observable and separable. The most significant state error cross correlations are within the orbit itself. Atmospheric density modeling errors are highly correlated with those of the orbit. This suggests that if atmospheric density errors are not estimated, then they will alias into and degrade the orbit estimate. Ballistic coefficient modeling errors are negligibly correlated with the orbit.

## 1 Introduction

A new prototype capability<sup>1</sup> has been developed to estimate ballistic coefficient error  $\Delta B/B$  and atmospheric density error  $\Delta\rho/\rho$  simultaneously in real-time. We demonstrate the sequential filter-smoother estimation of a spacecraft orbit, simultaneously with ballistic coefficient, atmospheric density, and other observable state parameters. Ballistic coefficient errors and atmospheric density errors are modeled as time-varying exponentially correlated Gauss-Markov sequences.

### 1.1 Filter-Smoother Description

The filter does input and process measurement data sequentially forward with time, and responds with a complete state estimate and error covariance within milli-seconds<sup>2</sup> of receipt of each measurement. This is what is meant here by *real-time*. It is enabled by accumulation of information from the infinite past, and by satisfaction of the requirements for optimal orbit determination<sup>3</sup>[13]. The real-time filtered state estimate and covariance are used as initial conditions for their forward propagation.

The smoother does input and process stored filter data sequentially backward with time, using the last filter state estimate and error covariance matrix, and associated epoch  $t_L$  as initial conditions. With decreasing time, the smoother input is defined by filter output together with recursively generated smoother output. Measurements are not reprocessed by the smoother. The smoothed state estimate is superior to the filtered state estimate for each time  $t_k < t_L$ . The smoother is thus not a real-time estimator.

### 1.2 New Results and Conclusions

Startling new results have been derived from the sequential processing of simulated and real AFSCN range data. The real range data was archived during the solar maximum in July 2000. This data time interval includes the Bastille Day geomagnetic storm and Coronal Mass Ejection (CME) on 14 July 2000. We claim to have demonstrated that:

---

\*© Analytical Graphics, Inc., 2004. Paper AAS 04-175 published by AAS/AIAA with permission.

<sup>1</sup>The state estimate structure for STK/OD has been extended to include the estimation of relative ballistic coefficient error  $\Delta B/B$ .

<sup>2</sup>This has been demonstrated on a PC.

<sup>3</sup>This paper can be viewed on line at: <http://www.stk.com/resources>. Under *Documentation* click *White Papers*.

- Ballistic coefficient and atmospheric density are simultaneously observable and separable in real-time estimation.
- Atmospheric density estimates and spacecraft position and velocity estimates satisfy McReynolds' filter-smoother consistency tests when the input 3-hourly  $a_P$  step functions are replaced by osculating polynomial splines. These tests fail when the 3-hourly  $a_P$  step functions are used.
- $K_P/a_P$  geomagnetic data with 3-hourly step functions are inadequate for optimal orbit determination.
- Cross correlations between the errors from sequentially *smoothed* estimates of ballistic coefficient and atmospheric density have significantly larger magnitudes than from sequentially *filtered* estimates.
- Atmospheric density estimation errors are highly correlated with orbit estimation errors. This suggests that if not estimated, atmospheric density modeling errors will alias into and degrade the orbit estimate.
- Ballistic coefficient estimation errors are negligibly correlated with orbit estimation errors.
- Filtered and smoothed estimates of ballistic coefficient are quite similar. Filtered and smoothed estimates of atmospheric density are quite different.
- The use of a time-constant model for ballistic coefficient ( $\tau_{\Delta B/B} = 1.0 \times 10^9$  min) with our *real* range data filter-smoother was shown to be invalid. See discussion in the Real Data section below.

### 1.3 Remarks

Failures of McReynolds' filter-smoother consistency tests, in the use of 3-hourly  $a_P$  step functions, prompt us to make the following coupled remarks:

- Complete raw magnetometer data, with a standard format, should be provided to the world community in addition to  $K_P/a_P$  data.
- New atmospheric density algorithms should be developed that appropriately model the complete raw magnetometer data.

### 1.4 Related Work

Our work here is a continuation of the effort described by Wright<sup>4</sup>[11] at the Puerto Rico meeting a year ago. The reader is referred to that paper for the following definitions of terms and related discussions:

- Definition of the stochastic baseline model and stochastic dynamic model for atmospheric density
- Definition of the exponential Gauss-Markov sequence model for both relative atmospheric density error  $\Delta\rho/\rho$  and relative ballistic coefficient error  $\Delta B/B$
- Use of  $K_P/a_P$  in Jacchia's[1] 1971 global atmospheric density model

McReynolds' rigorous filter-smoother consistency test is defined in Wright[13]. The current paper by Wright and Tanygin (AAS 04-176)[12] details the removal of arbitrary discontinuities in atmospheric density modeling, using osculating polynomial splines to smooth  $a_P$  discontinuities.

### 1.5 Orbit Elements

Initial epoch of real data: 1 July 2000 00:00:00.0 UTC (solar maximum). Initial epoch of simulated data: 1 September 2003 00:00:00.0 UTC (not solar maximum). Initial orbit values for both the real data and simulated data computer runs:  $a = 1.0778er$ ,  $e = 0.00046$ ,  $i = 105.026$  deg,  $\Omega = 350.724$  deg,  $\omega = 237.826$  deg.

---

<sup>4</sup>This paper can be viewed on line at: <http://www.stk.com/resources>. Under *Documentation* click *White Papers*.

It is important to note that graphics derived from smoother products, presented in that paper, were contaminated by unfortunate 3-hour step functions due to overlapping smoother executions with 3-hour (180 min) overlaps. For the smoother object in computer runs referred to herein,  $IntervalLength = 525960$  min (1 year), and  $IntervalOverlap = 0$  min.

## 2 Air Drag Acceleration Error Model

The perturbative air-drag acceleration  $\ddot{z}_D$  has the form:

$$\ddot{z}_D = -\frac{1}{2}B\rho\dot{s}^2K \quad (1)$$

where:

$$B = \frac{C_D A}{m} \quad (2)$$

where  $\ddot{z}_D$  is a  $3 \times 1$  perturbative drag acceleration matrix with inertial components,  $C_D$  is the unitless drag coefficient,  $A$  is the spacecraft area projection onto a plane orthogonal to the spacecraft velocity vector  $\dot{\mathbf{s}}$  referred to a rotating Earth,  $\dot{s}$  is the length of  $\dot{\mathbf{s}}$ ,  $m$  is spacecraft mass,  $\rho$  is atmospheric density, and  $K$  is a  $3 \times 1$  unit matrix that contains inertial components of  $\dot{\mathbf{s}}/\dot{s}$ .

The estimation errors  $\Delta\ddot{z}_D$  in LEO air-drag accelerations  $\ddot{z}_D$  are due most significantly to random errors in modeled atmospheric density  $\rho$  and ballistic coefficient  $B$ . Differentiation of Eq. 1 provides:

$$\Delta\ddot{z}_D = \left( \frac{\Delta B}{B} + \frac{\Delta\rho}{\rho} \right) \ddot{z}_D \quad (3)$$

an associated instantaneous error model. We model both  $\Delta B/B$  and  $\Delta\rho/\rho$  as exponentially correlated Gauss-Markov sequences. When their exponential half-life times are significantly different, then they can be estimated simultaneously. There is a significant subset of real LEOs for which this is true. We address this subset.

### 2.1 Gauss-Markov Exponential Half-Life Values

Denote the Gauss-Markov exponential half-life values by  $\tau_{\Delta\rho/\rho}$  for atmospheric density and  $\tau_{\Delta B/B}$  for ballistic coefficient. Then for the simulated data run:  $\tau_{\Delta\rho/\rho} = 180$  min and  $\tau_{\Delta B/B} = 1.0 \times 10^9$  min ( $\sim \infty$ ), and for the real data run:  $\tau_{\Delta\rho/\rho} = 200$  min and  $\tau_{\Delta B/B} = 10080$  min (*7days*).

### 2.2 Covariance Trigger Function on Atmospheric Density

Fig. 42 displays the 3-hourly step functions in  $a_P$  values associated with magnetometer response to the Bastille Day geomagnetic storm. It also displays Jacchia's[1] mean lag estimate (6.7hr) between magnetometer measurement and atmospheric density response. The a priori modeled atmospheric density responds also with 3-hourly step functions. The Fig. 43 cartoon illustrates 3-hourly step functions in  $a_P$ , and the use of polynomial splines to remove the discontinuities.

A user defined relative atmospheric density increase threshold  $T_{AD}$  is designed to autonomously trigger an increase in the variance in atmospheric density error  $\Delta\rho/\rho$ , during filtering, when a relative increase in modeled atmospheric density exceeds the threshold[11]. Step functions in atmospheric density due to step functions in  $a_P$  trigger the filter variance increase. When  $a_P$  3-hourly discontinuous step functions are used, we have set  $T_{AD} = 0.10$ . When  $a_P$  splines are used, we have set  $T_{AD} = 0.01$ . Use of this trigger function, when splined values of  $a_P$  are used, generates a discretization of the filter atmospheric density error covariance input even though the  $a_P$  splines are smooth.

## 3 Simulated Data

The use of simulated truth orbits and realistic simulated measurement data has a very significant advantage over real data: Both filtered and smoothed state estimates can be compared to the known simulated truth. Simulation enables an important part of the algorithm and software validation effort, it enables comparison of estimation errors to associated  $0.95P$  ( $2\sigma$ ) error boundaries, and it provides a visual characterization of estimated filter and smoother functions with respect to simulated truth functions.

### 3.1 Ballistic Coefficient and Atmospheric Density

We have demonstrated here that estimates of ballistic coefficient and atmospheric density are simultaneously observable and separable in real-time estimation.

### 3.1.1 Atmospheric Density Estimates

Inspect Fig. 2 to see that the smoothed estimate of atmospheric density is indeed a useful *smoothed* estimate function, in phase with the simulated truth. Inspect Fig. 1 to see that the filtered estimate lags the truth, and seems to be a poor estimate function in its magnitude as compared to the smoothed estimate. Inspect Fig. 3 to compare the filtered and smoothed estimates directly.

Since smoother inputs consist only of filter outputs, it is helpful to recall that each smoothed estimate derives from measurement information both before and after the smoothed estimate, whereas each filtered estimate derives from measurement information only before the filtered estimate. Then only the smoothed estimate of atmospheric density should be used directly for knowledge of atmospheric density (science applications). The filtered estimate of atmospheric density provides a place in the state estimate to put the observable part of atmospheric density so that it will not corrupt the real-time orbit estimate, nor the orbit propagation derived from the real-time orbit estimate (military applications).

Fig. 4 presents the atmospheric density differences (errors) between simulations and smoothed estimates, together with appropriate  $0.095P$  ( $2\sigma$ ) error boundaries. It is only with simulated data that estimate errors can be constructed, because error knowledge depends on knowledge of the truth. The differences here are smoothed estimate *errors*, and the  $2\sigma$  error boundaries refer to these differences.

In contrast to this, when  $2\sigma$  *error* boundaries are overlayed with *estimates*, there is no expectation that the *estimates* will be bounded by their estimate *error* boundaries. See Fig. 6 for a ballistic coefficient example that makes this clear.

### 3.1.2 Ballistic Coefficient Estimates

The Gauss-Markov exponential half-life value for ballistic coefficient  $\tau_{\Delta B/B} = 1.0 \times 10^9$  min enabled a demonstration that the Gauss-Markov sequence simulation can be used effectively to model a time-constant. See Figs. 5 through 8. But the time-constant model may not be advisable for real data, as discussed below.

## 4 Real Data

Our tracking data consists of real range data from 14 AFSCN ground stations during July 2000, a time interval at solar maximum that includes the response to a massive CME that struck the Earth. The range data is dense within each station pass of a few minutes. But there are significant time intervals with no data between station passes. See Fig. 9 for a typical distribution of range data residuals from station BOSS-A (New Hampshire).

### 4.1 Optimal Orbit Determination

Optimal orbit determination[13] demands unbiased Gaussian range residuals and the satisfaction of McReynolds' rigorous Filter-Smoother Consistency Test.

#### 4.1.1 White-Noise Range Residuals

Figs. 10 through 13 demonstrate white-noise range residuals.

#### 4.1.2 McReynolds' Filter-Smoother Consistency Tests and $a_P$ Step Functions

For each parameter of the state estimate, a unitless ratio is formed. The ratio-numerator consists of the difference between filtered and smoothed state estimate at a common time. The ratio-denominator consists of a root-variance (sigma) on the numerator difference, derived from the filtered and smoothed state estimate error covariance function. Each state parameter ratio can be graphed as a function of time. McReynolds' Filter-Smoother Consistency Test consists in comparing this unitless ratio to  $\pm 3$ . If 99% of the ratios graphed fall between  $-3$  and  $3$ , then the test is defined a success<sup>5</sup>. If not, the test is defined a failure.

Initialization of the sequential filter requires the processing of measurement data across the filter initialization time interval. Since initialization is required to develop realistic covariance elements, the Filter-Smoother Consistency Test is ignored during filter initialization.

---

<sup>5</sup>The bases for this test consist of the use of the Normal density function for state estimation error modeling, extensive experience with comparisons of error modeling with the Normal density function, and the Central Limit Theorem.

Figs. 28 and 29 show satisfaction<sup>6</sup> of McReynolds' Filter-Smoother Consistency Test[13] in atmospheric density and spacecraft position when input values of  $a_P$  are splined<sup>7</sup> (smoothed) before use<sup>8</sup>. Figs. 26 and 27 show failure of the Filter-Smoother Consistency Test when 3-hourly step functions of  $a_P$  are used.

So we have shown that the 3-hourly step functions in  $a_P$  lead to very poor performance. And we have shown that the smoothed integral-preserving  $a_P$  splines lead to acceptable performance. But we selected the simplest osculating polynomial splines for these runs. We could just as well have selected different smooth splines[12]. We have no way to know how to approximate the actual magnetometer measurements. It is thus remarkable that replacement of the 3-hourly  $a_P$  step functions with these smoothed  $a_P$  splines produces such a dramatic improvement in McReynolds' Filter-Smoother Consistency Test.

## 4.2 Ballistic Coefficient and Atmospheric Density Estimates

Ballistic coefficient  $\Delta B/B$  and atmospheric density  $\Delta\rho/\rho$  are simultaneously observable and separable in real-time estimation. The figures referred to in this paragraph all derive from the real range data run using  $a_P$  splines. Figs. 14 and 15 display filter and smoother estimates in atmospheric density between 0 MAM and 37000 MAM (Minutes After Midnight of the initial epoch). Figs. 16 and 17 display filter and smoother estimates in atmospheric density between 18000 MAM and 22400 MAM. Figs. 20 and 21 display filter and smoother estimates in atmospheric density between 21660 MAM and 21780 MAM, a two-hour interval.

Fig. 22 displays the smoother estimates in atmospheric density between 21660 MAM and 21780 MAM, but it derives from a real range data run using the nominal 3-hourly step function discontinuities in  $a_P$ . Compare Figs. 21 and 22 to see the comparative effect of  $a_P$  splines across this dynamic interval. Use of the  $a_P$  splines has reduced the amplitude of estimates in  $\Delta\rho/\rho$ , and has spread out the total area; i.e., splines in  $a_P$  have spread out the integral of the smoothed estimates of  $\Delta\rho/\rho$ .

### 4.2.1 Separability Evident in Cross-Correlations

If atmospheric density errors and ballistic coefficient errors were perfectly correlated (cross-correlation =  $\pm 1$ ), then the estimator could not distinguish them. To see that this is not the case, see Figs. 30 and 31.

### 4.2.2 Contrasts

Filtered and smoothed estimates of ballistic coefficient are quite similar: Compare Figs. 24 and 25. Filtered and smoothed estimates of atmospheric density are quite different: Compare Figs. 16 and 17; and compare Figs. 20 and 21.

## 4.3 Cross-Correlations within the State Estimate

The graphics referred to in this section display cross-correlations derived from the state error covariance function during the 26 days of real range measurement processing. It is easy to demonstrate[9] that:  $-1 \leq \text{cross-correlation} \leq 1$ . When two parameters are perfectly correlated (cross-correlation =  $\pm 1$ ), then the estimator cannot distinguish the estimates for the two parameters. When two parameters are highly correlated (cross-correlation near  $\pm 1$ ) and one of them *is* included in the state estimate structure and one of them is *not* included in the state estimate structure, then the estimator will alias the effects of the unestimated parameter into the parameter that is estimated. Knowledge of state estimate cross-correlations relates intimately to the requirement for a complete state estimate structure for optimal orbit determination[13].

### 4.3.1 Orbit Estimate Errors

Figs. 40 and 41 display cross-correlations within the orbit estimate. Orbit estimate errors seem always to be extremely correlated<sup>9</sup> in this manner.

<sup>6</sup>We ignore violations that occur during the filter initialization time interval.

<sup>7</sup>A similar technique has been suggested by Sabol and Luu[14].

<sup>8</sup>McReynolds' Filter-Smoother Consistency Test is not satisfied during the filter initialization interval.

<sup>9</sup>One sees here the extreme linear dependencies within the orbit covariance matrix function. The orbit covariance matrix is always extremely ill-conditioned. There are no matrix inversions required by the filter, so this is not a problem for the filter. The smoother does require matrix inversions. This subject must be addressed in a separate study.

### 4.3.2 Atmospheric Density and Ballistic Coefficient Estimate Errors

Figs. 30 and 31 display cross-correlations between atmospheric density errors and ballistic coefficient errors. Cross correlations between the errors from sequentially *smoothed* estimates of ballistic coefficient and atmospheric density have significantly larger magnitudes than from sequentially *filtered* estimates. The most significant correlations in filtering occur during filter initialization. This facilitates unwanted aliasing between atmospheric density estimates and ballistic coefficient estimates during filter initialization, and explains the disastrous results incurred during the computer run referred to below (Modeling the Ballistic Coefficient as a Time Constant).

### 4.3.3 Atmospheric Density and Orbit Estimate Errors

Figs. 32 through 35 display cross-correlations between atmospheric density errors and orbit estimate errors. This provides the most convincing reasons for estimating atmospheric density: Provide a place in the state estimate to absorb atmospheric density modeling errors so they do not alias into the orbit estimate.

### 4.3.4 Ballistic Coefficient and Orbit Estimate Errors

Figs. 36 through 39 display cross-correlations between ballistic coefficient errors and orbit estimate errors. When atmospheric density is simultaneously estimated with the ballistic coefficient, then the estimated ballistic coefficient estimate errors are negligibly correlated to the orbit.

## 4.4 Modeling the Ballistic Coefficient as a Time Constant

If the unknown spacecraft ballistic coefficient were a time-constant, then the estimation of this time constant would provide a tremendous trajectory accuracy advantage in the propagation of state estimate and error covariance functions. This motivated our computer run to model the ballistic coefficient as a time constant in the filter-smoother processing of real range data (also see our simulation results). A time-constant is very well approximated with an exponential Gauss-Markov function by setting its exponential half-life value to a very large number.

The Gauss-Markov exponential half-life value  $\tau_{\Delta B/B} = 1.0 \times 10^9$  min ( $\sim \infty$ ) was applied to the one-month span of V3333 real range data with disastrous results in the sequential filter. Atmospheric density aliased into ballistic coefficient during filter initialization and stayed there. This was facilitated by cross-correlations between atmospheric density errors and ballistic coefficient errors during the filter initialization interval.

## 4.5 Filter Over-Corrections

The V3333<sup>10</sup> range data was provided<sup>11</sup> in response to our request for worst case experience with operational LEO orbit determination. Figure 23 identifies a difficulty with the unique circumstances of this station ranging data: After the long propagation intervals between some station passes, the first filter correction to atmospheric density is a significant over-correction. Here the filter gain on atmospheric density is wide open<sup>12</sup> due to covariance propagation and drag acceleration error accumulation, and due to extreme solar activity during this interval at solar maximum. The filter over-correction was not removed by the smoother. We have not observed this problem with station ranging except under this combination of extreme conditions. We expect to demonstrate the absence of this problem when we process GPS measurements distributed densely and uniformly about the orbit.

## 5 Looking Forward

It remains to demonstrate the estimation of global real-time atmospheric density, simultaneously with local atmospheric density and ballistic coefficient. Observability for global estimation will require tracking measurements from an ensemble of LEOs, preferably massive spacecraft with spherical bodies.

When the exponential half-life of the ballistic coefficient  $\tau_{\Delta B/B}$  is significantly longer than that of atmospheric density  $\tau_{\Delta \rho/\rho}$ , we expect to show in a future study that orbit propagation accuracies depend significantly on  $\tau_{\Delta B/B}$ .

---

<sup>10</sup>Also known as LEOh497.

<sup>11</sup>This data was provided by Tom Gidlund and the AFSCN.

<sup>12</sup>The effect of reducing the variance/gain on atmospheric density is to violate McReynolds' filter-smoother consistency test before the reduction eliminates the overcorrection.

**Acknowledgement 1** *We appreciate the technical reviews by Richard Hujzak, William Chuba, Tom Johnson, Sal Alfano, and David Vallado.*

## References

- [1] L. G. Jacchia, *Revised Static Models of the Thermosphere and Exosphere with Empirical Temperature Profiles*, Smithsonian Astrophysical Observatory, Special Report 332, 1971
- [2] The Committee for the CIRA Working Group 4, *COSPAR International Reference Atmosphere 1972 (CIRA 1972)*, Akademie-Verlag, Berlin, 1972
- [3] L. G. Jacchia, *New Static Models of the Thermosphere and Exosphere with Empirical Temperature Profiles*, Smithsonian Astrophysical Observatory, Special Report 313, 1970
- [4] L. G. Jacchia, *Thermospheric Temperature, Density, and Composition: New Models*, Smithsonian Astrophysical Observatory, SAO Special Report 375, 1977
- [5] Sherman, S., *A Theorem on Convex Sets with Applications*, Ann. Math. Stat., 26, 763-767, 1955.
- [6] Sherman, S., *Non-Mean-Square Error Criteria*, IRE Transactions on Information Theory, Vol. IT-4, 1958.
- [7] Kalman, R. E., *New Methods in Wiener Filtering Theory*, Proceedings of the First Symposium on Engineering Applications of Random Function Theory and Probability, edited by J. L. Bogdanoff and F. Kozin, John Wiley & Sons, New York, 1963.
- [8] Rauch, H. E., *Solutions to the Linear Smoothing Problem*, IEEE Trans. Autom. Control, vol. AC-8, p. 371, 1963
- [9] Meditch, J. S., *Stochastic Optimal Linear Estimation and Control*, McGraw-Hill, New York, 1969.
- [10] Bruce R. Bowman, *True Satellite Ballistic Coefficient Determination for HASDM*, Paper AIAA 2002-4887, AIAA/AAS Astrodynamic Specialist Conference, 5-8 August 2002, Monterey, CA.
- [11] James R. Wright, *Real-Time Estimation of Local Atmospheric Density*, Paper AAS 03-164, 13<sup>th</sup> AAS/AIAA Space Flight Mechanics Meeting, Ponce, Puerto Rico, 9-13 February 2003.
- [12] James R. Wright, Sergei Tanygin, *Removal of Arbitrary Discontinuities in Atmospheric Density Modeling*, 14<sup>th</sup> AAS/AIAA Space Flight Mechanics Conference, Maui, Hawaii, 8-12 February 2004.
- [13] James R. Wright, *Optimal Orbit Determination*, Paper AAS 02-192, AAS/AIAA Space Flight Mechanics Meeting, San Antonio, Texas, 27-30 Jan., 2002.
- [14] Chris Sabol, K. Kim Luu, *Atmospheric Density Dynamics and the Motion of Satellites*, Air Force Research Laboratory, Directed Energy Directorate, 535 Lipoa Parkway, Suite 200, Kihei, HI 96753, Paper given: 2002 AMOS Technical Conference, Wailea, HI, Sept. 2002

## 6 Graphics

Simulated range data results are presented in Figs. 1 through 8. Real range data results are presented in Figs. 9 through 41. Except for Histograms, the abscissa (X axis) of each graph presents the number of minutes after initial epoch for the computer run. For example, for real range data results, to convert any time value from units *minutes* to *date* (with day fraction) in July 2000, divide by 1440 and add 1.

## 6.1 Simulated Range Data

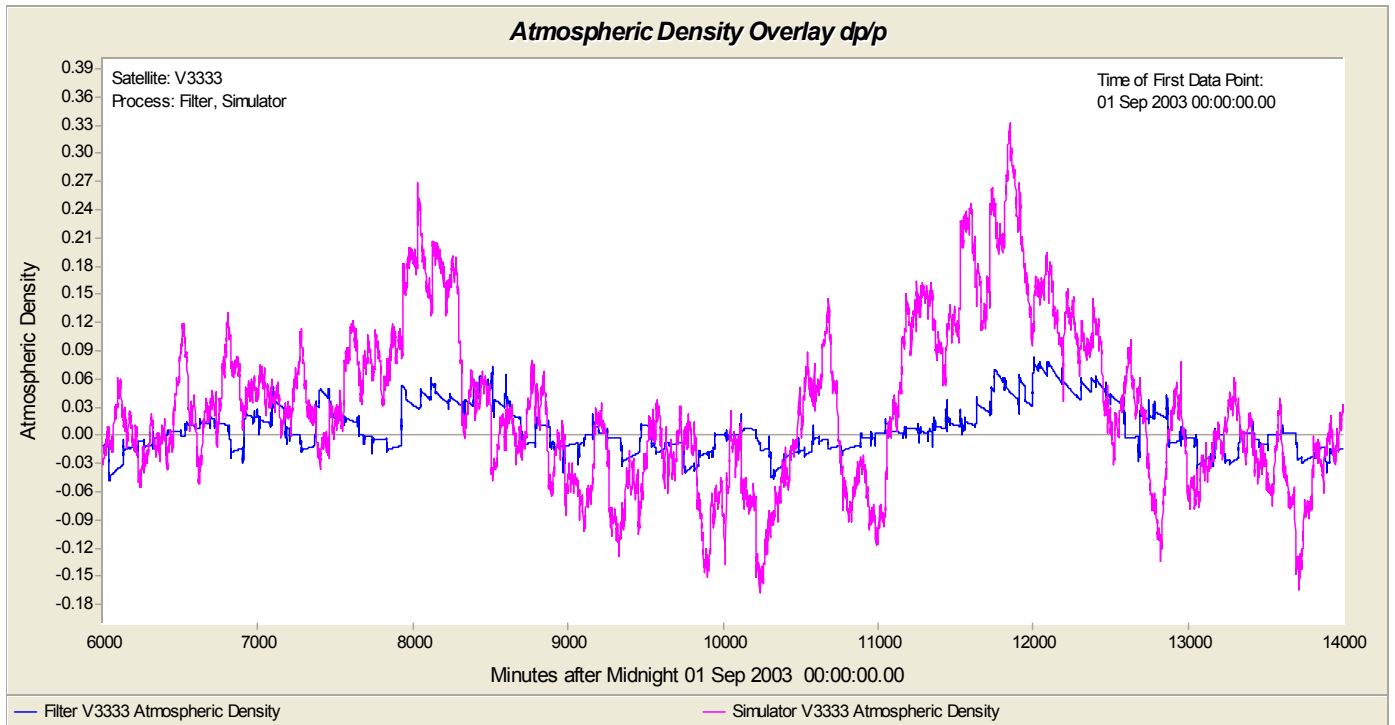


Figure 1: Overlay Atmospheric Density  $\Delta\rho/\rho$ : Simulated and Filtered (simDATA)

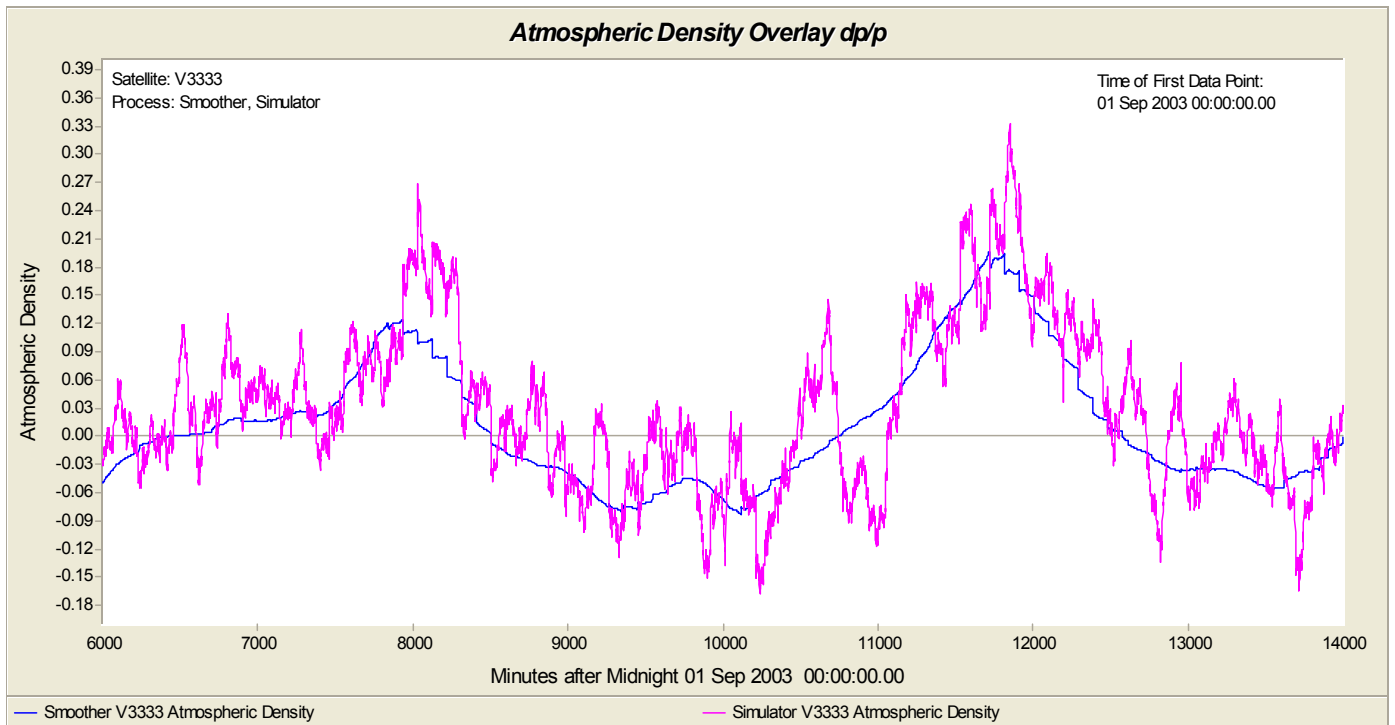


Figure 2: Overlay Atmospheric Density  $\Delta\rho/\rho$ : Simulated and Smoothed (simDATA)



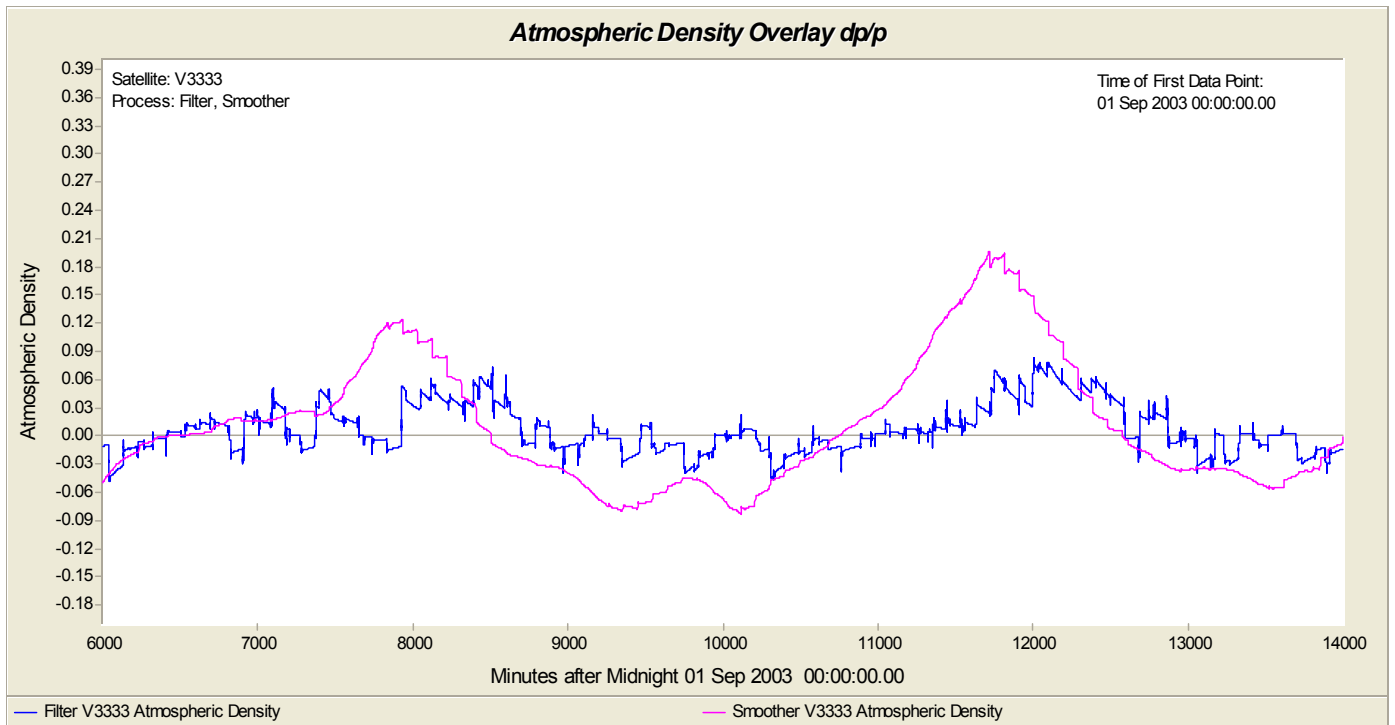


Figure 3: Overlay Atmospheric Density  $\Delta\rho/\rho$ : Filtered and Smoothed (simDATA)

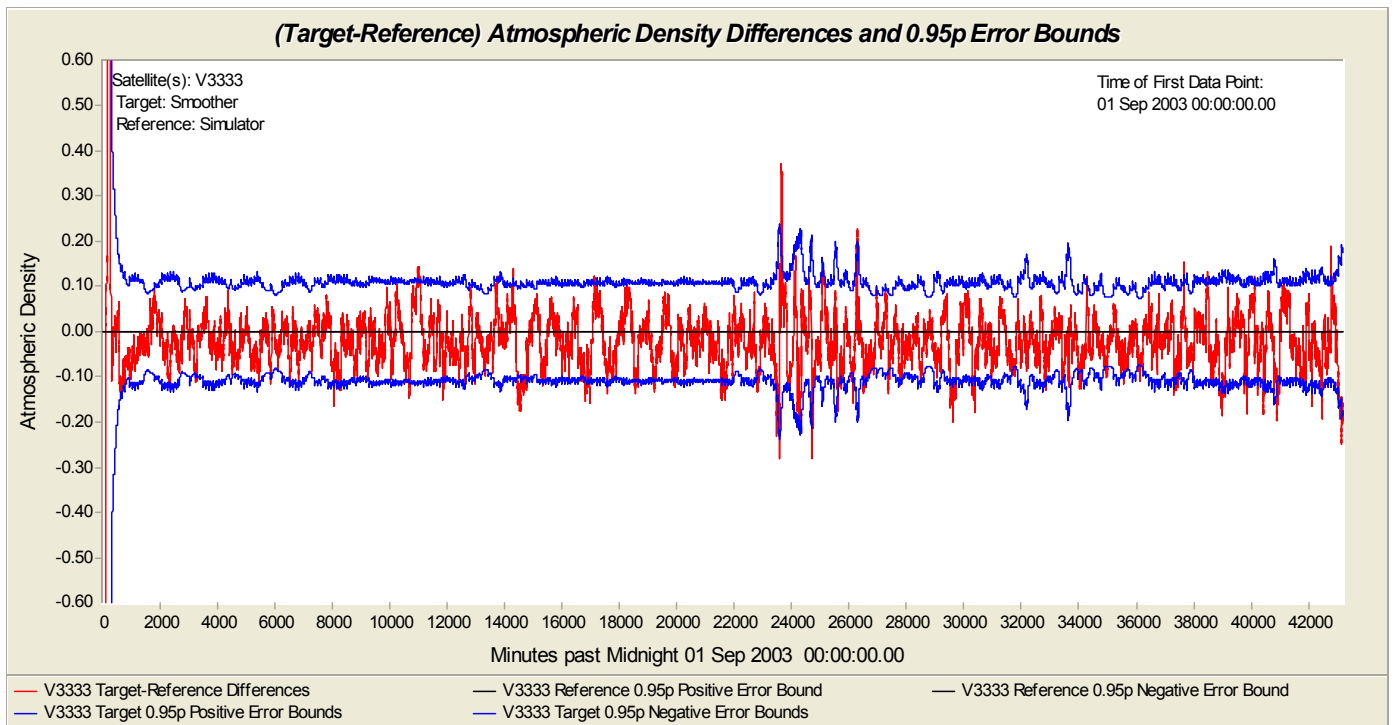


Figure 4: Atmospheric Density  $\Delta\rho/\rho$  Difference, Simulated less Smoothed (simDATA)

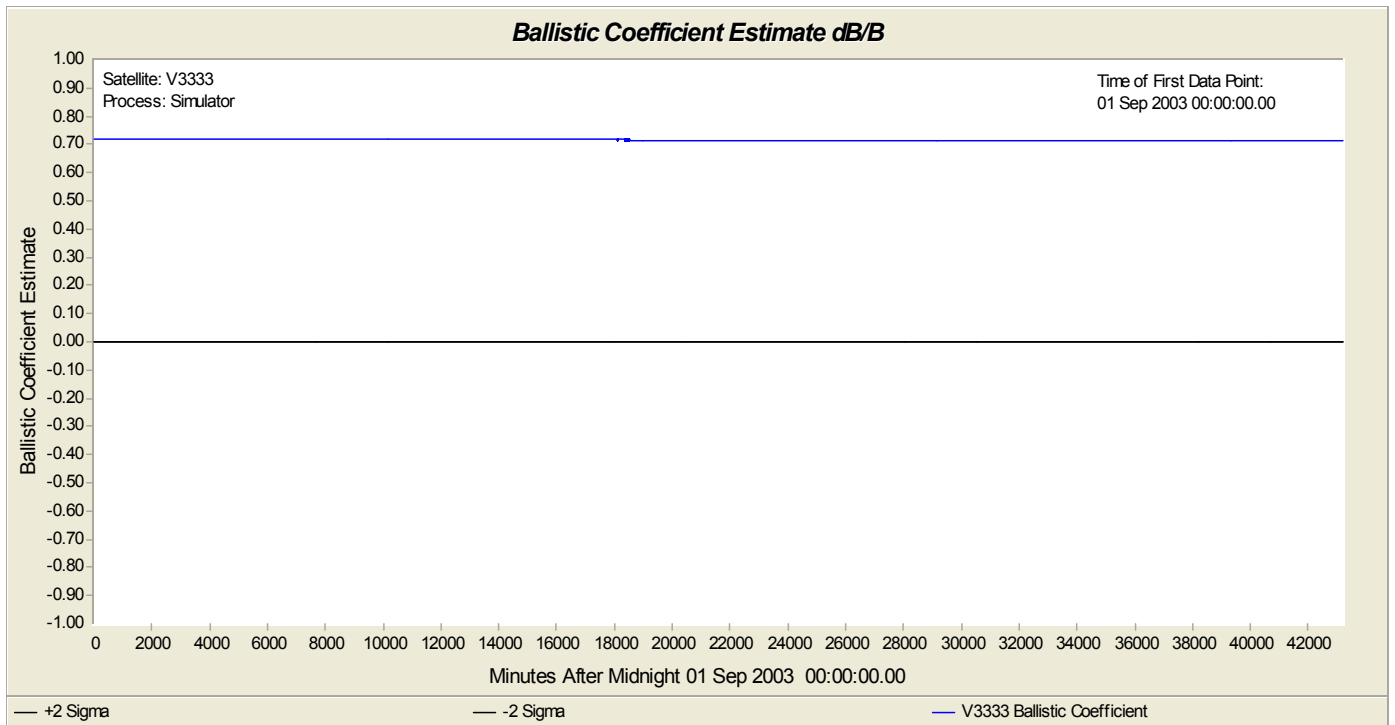


Figure 5: Simulated Ballistic Coefficient  $\Delta B/B$  (simDATA)

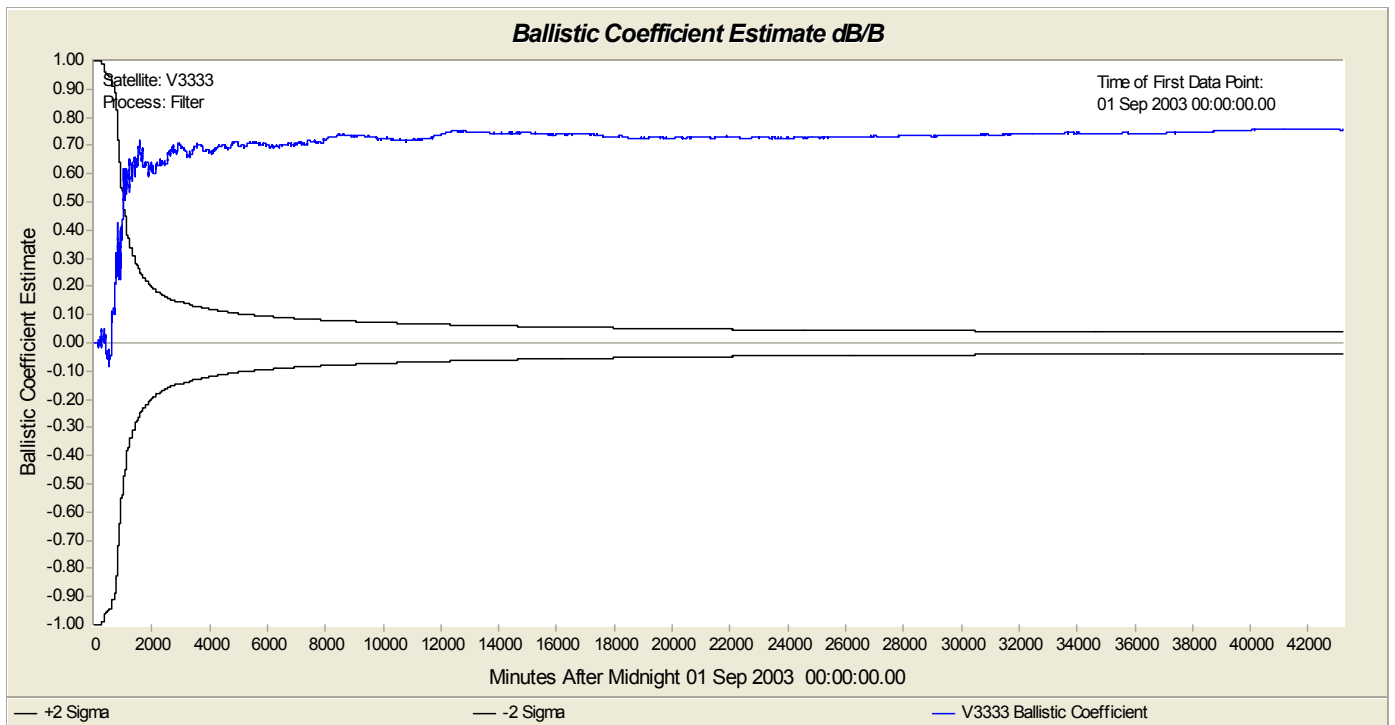


Figure 6: Filtered Estimate of the Ballistic Coefficient  $\Delta B/B$  (simDATA)

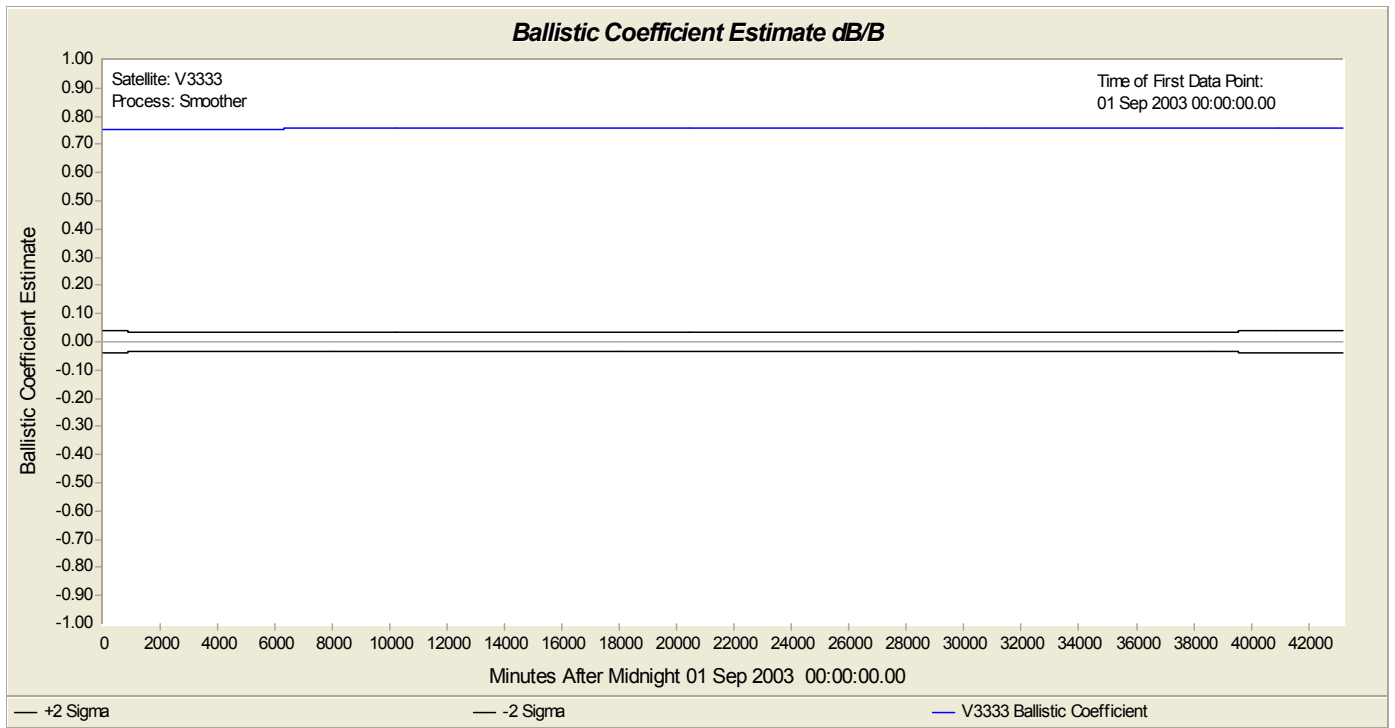


Figure 7: Smoothed Estimate of the Ballistic Coefficient  $\Delta B/B$  (simDATA)

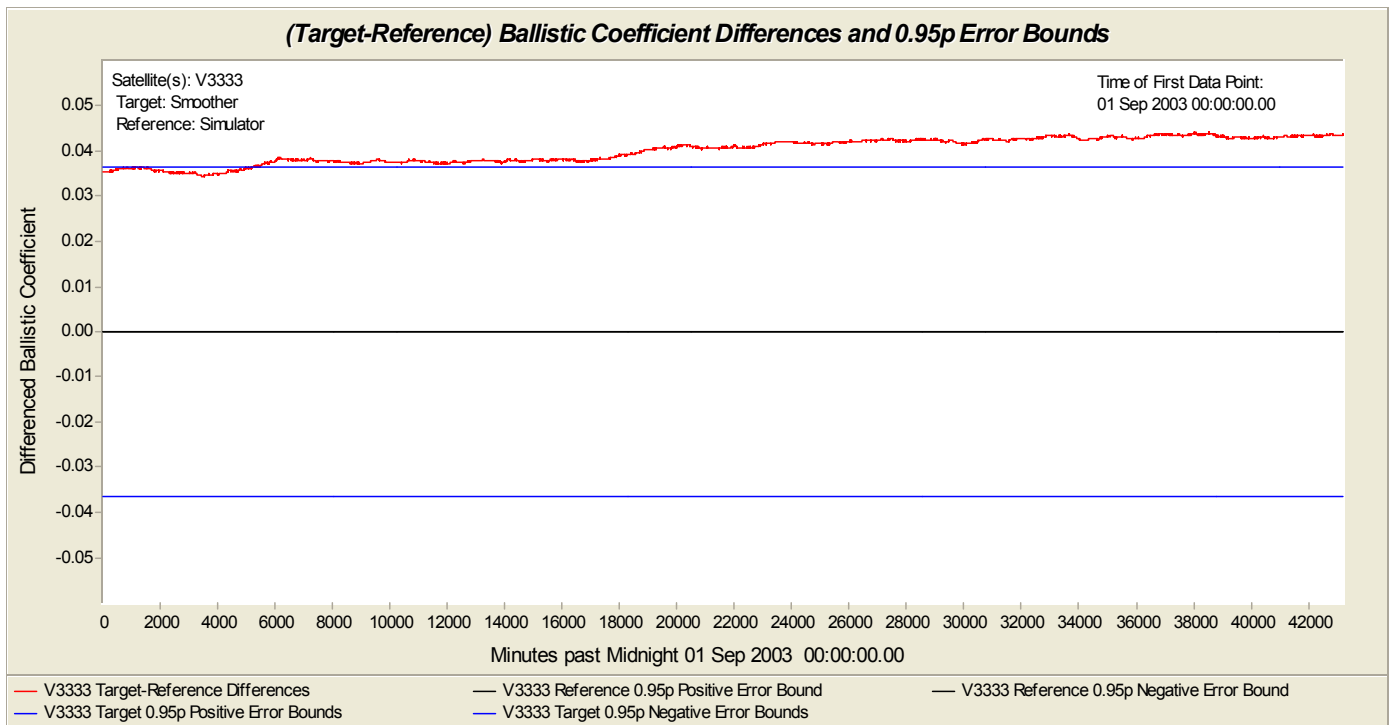


Figure 8: Ballistic Coefficient  $\Delta B/B$  Difference, Simulated less Smoothed (simDATA)

## 6.2 Real Range Data

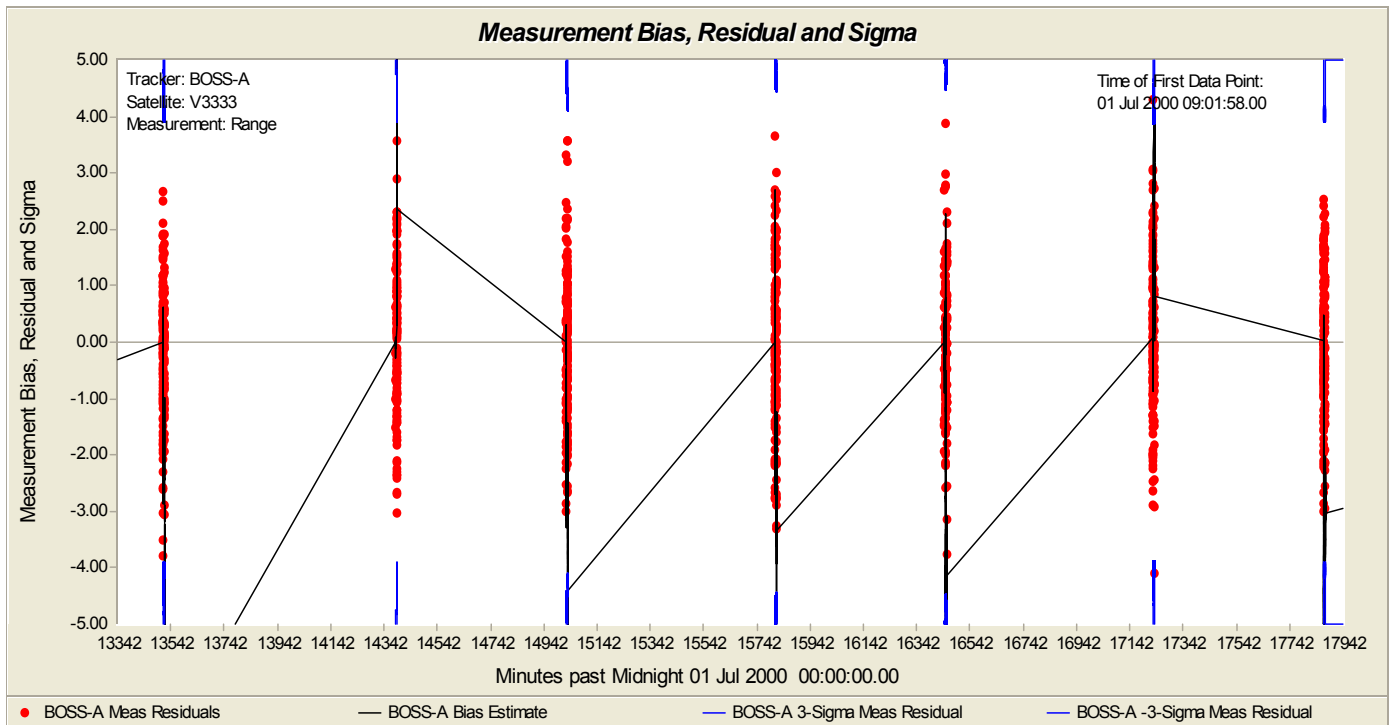


Figure 9: Real Range Residuals for 7 BOSS-A Passes

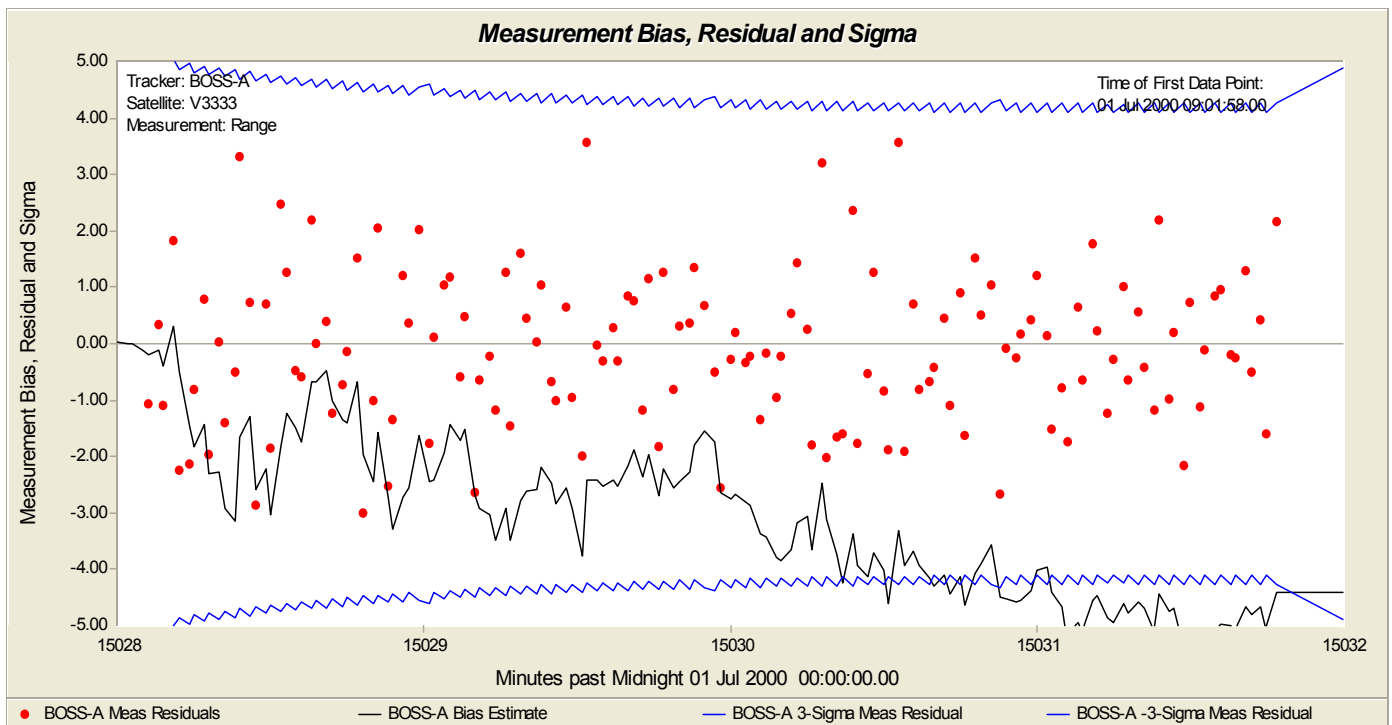


Figure 10: Range Residuals, Edit Thresholds, Bias Estimates, Pass Start 15028

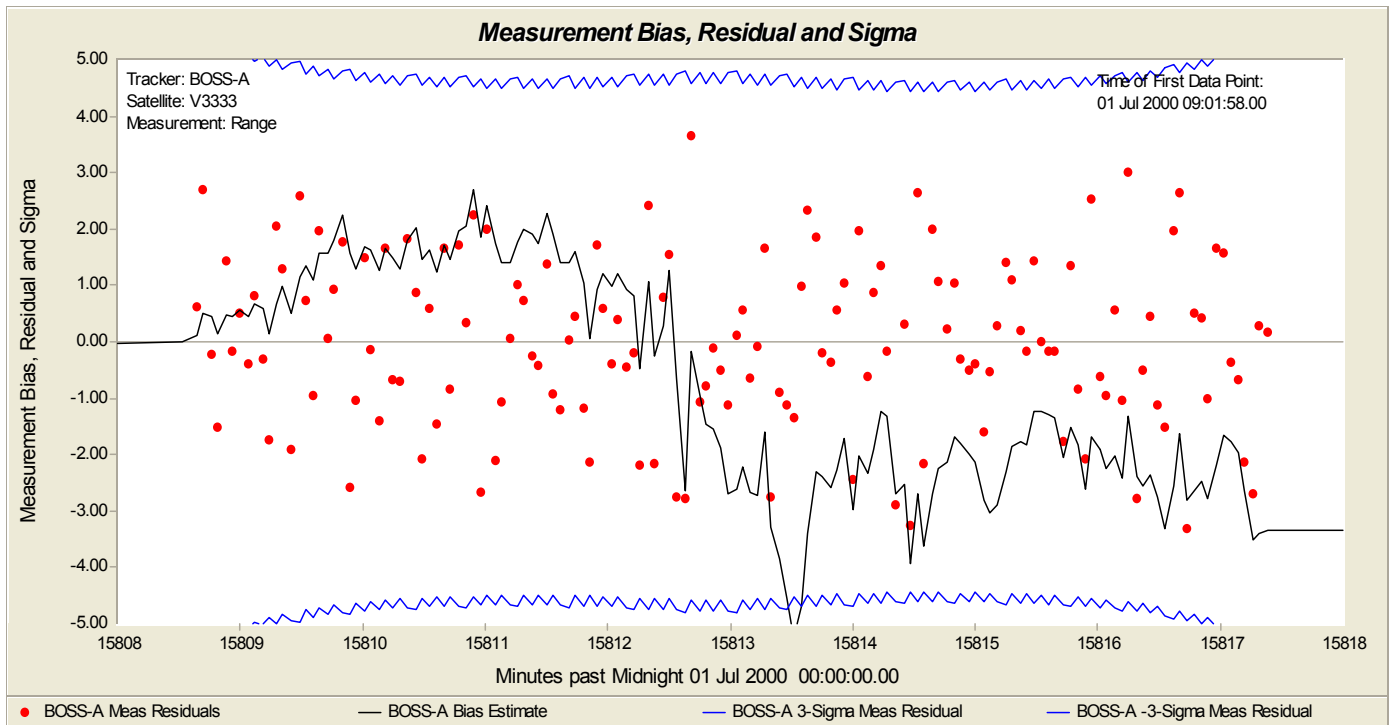


Figure 11: Range Residuals, Edit Thresholds, Bias Estimates, Pass Start 15808

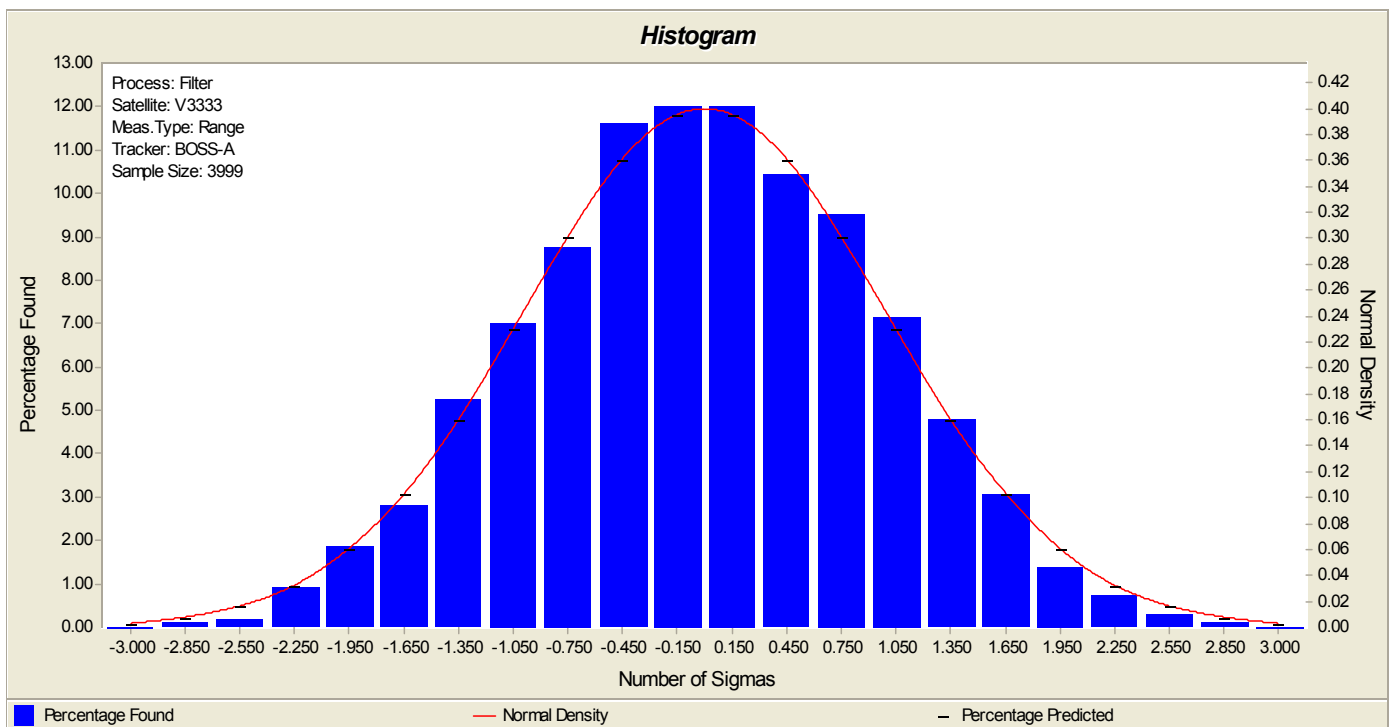


Figure 12: BOSS-A Range Residual Ratio Histogram

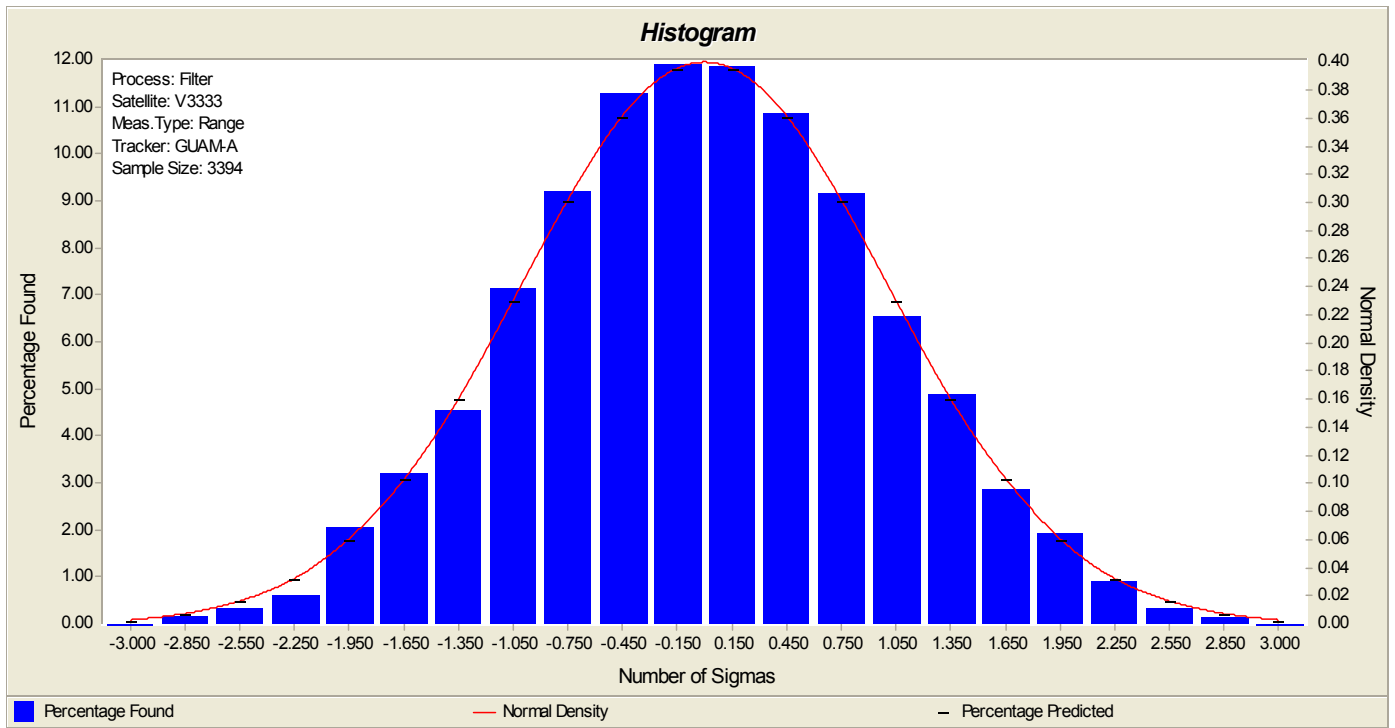


Figure 13: GUAM-A Range Residual Ratio Histogram

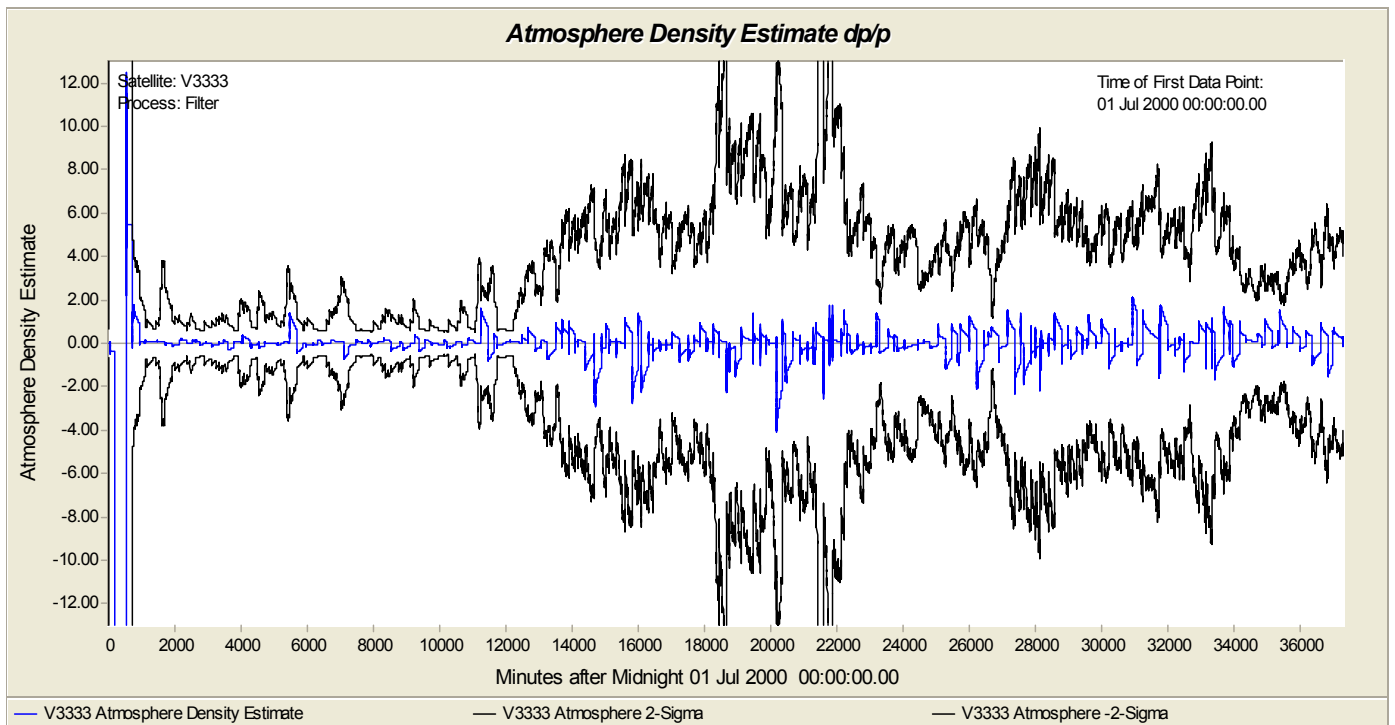


Figure 14: 26 Day Filter Atmospheric Density Estimate  $\Delta\rho/\rho$  & Error Covariance Envelope ( $2\sigma$ )

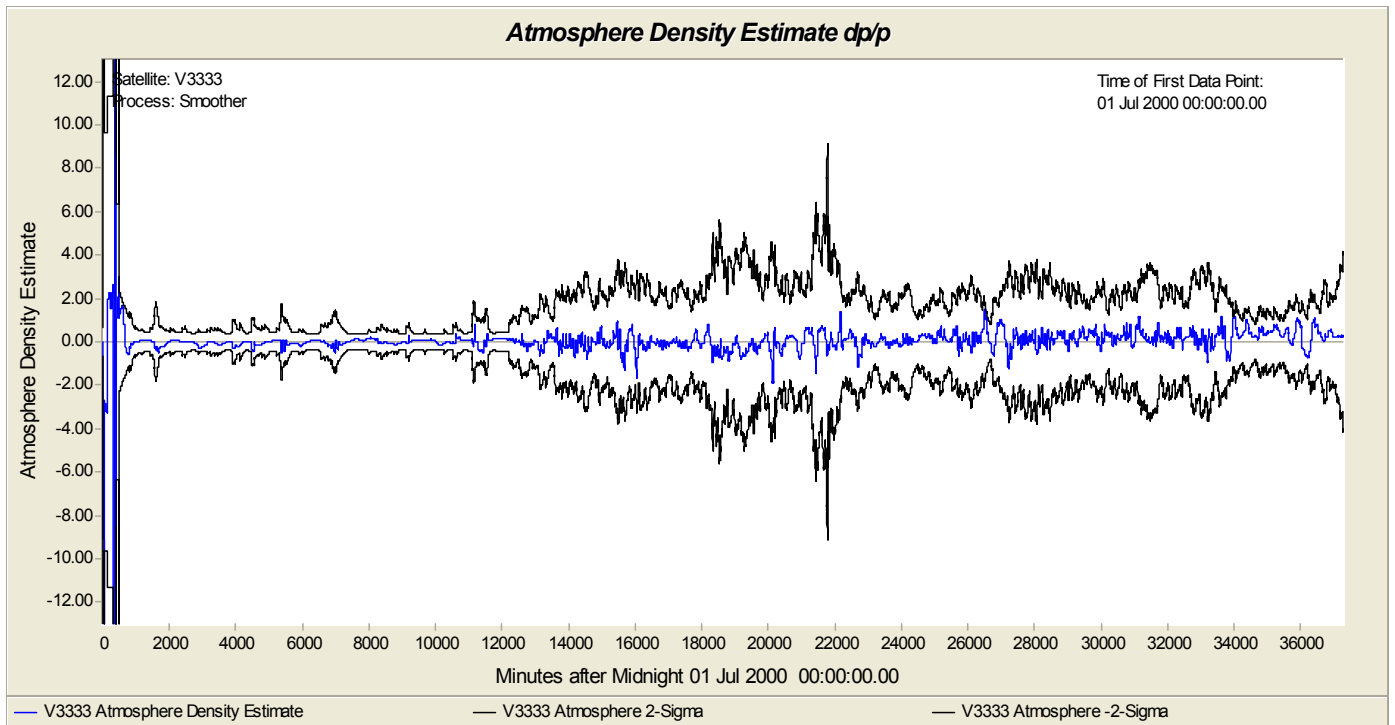


Figure 15: 26 Day Smoother Atmospheric Density Estimate  $\Delta\rho/\rho$  & Error Covariance Envelope ( $2\sigma$ )

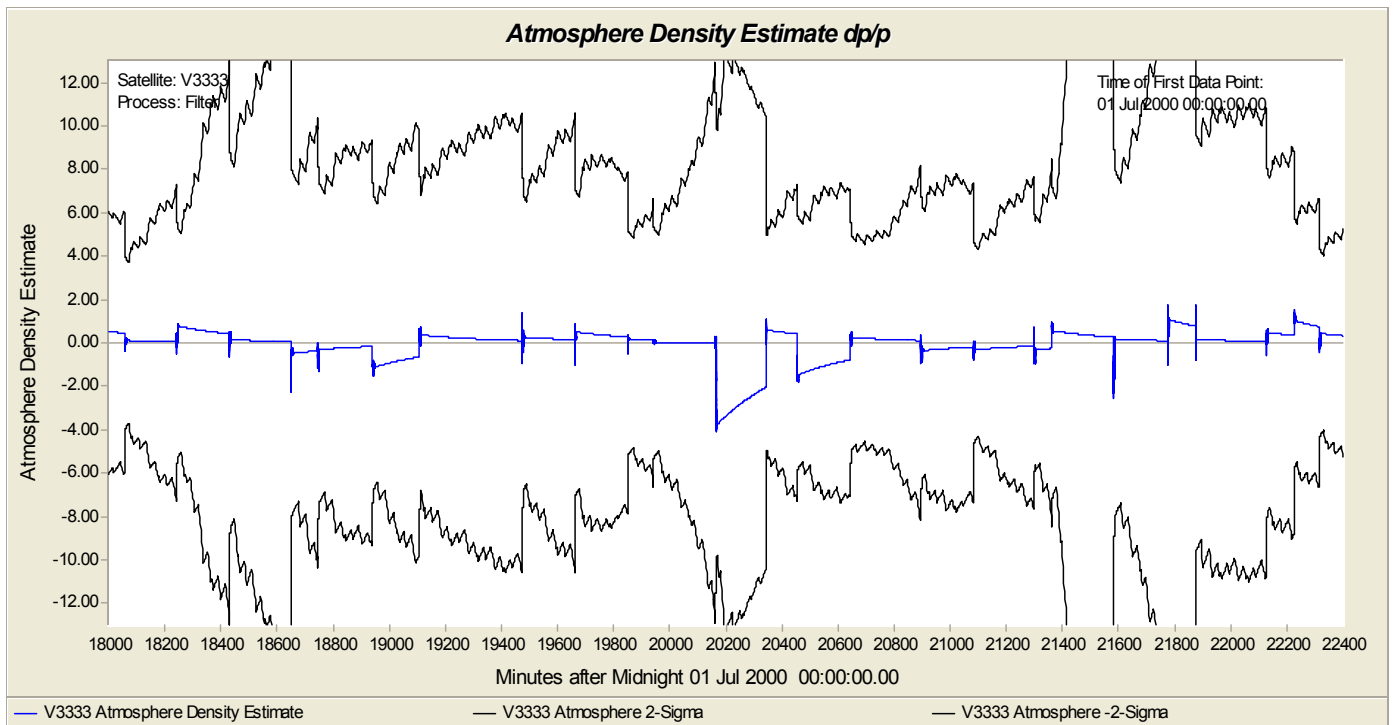


Figure 16: 3 Day Filter Atmospheric Density Estimate  $\Delta\rho/\rho$  & Error Covariance Envelope ( $2\sigma$ )

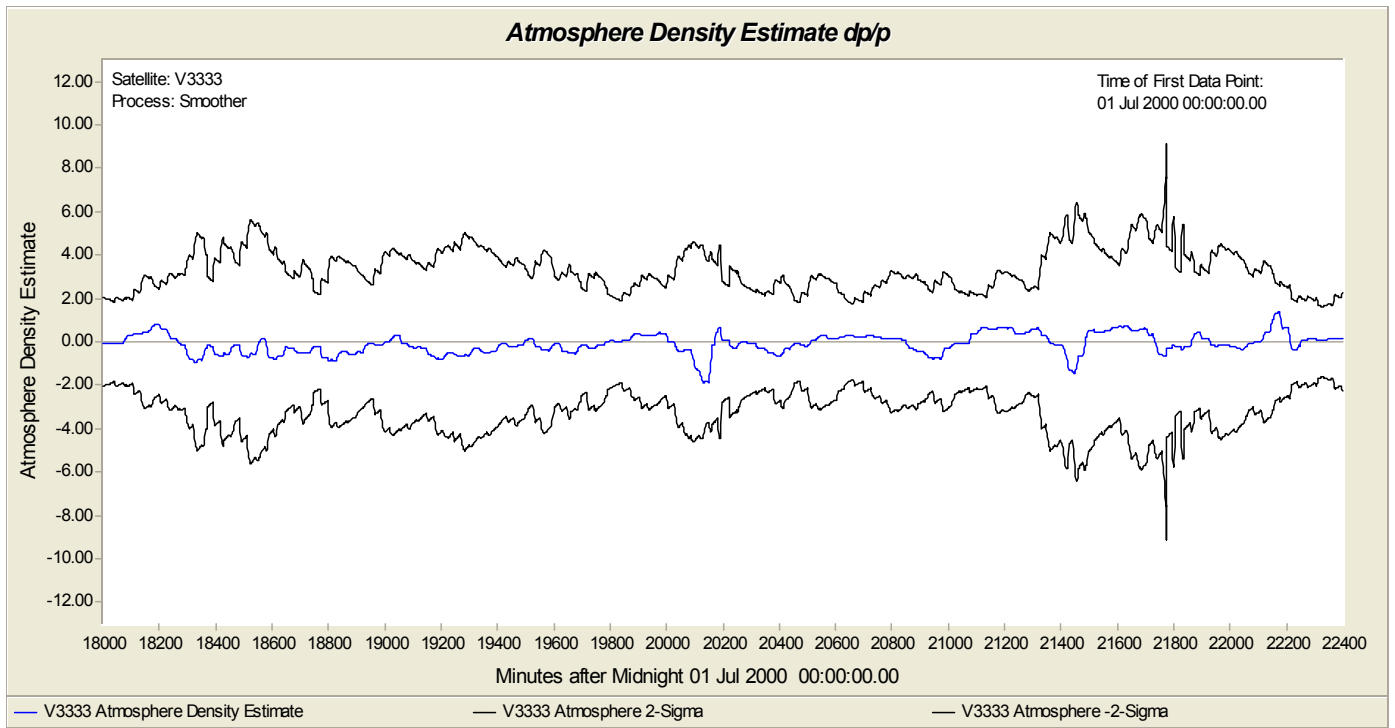


Figure 17: 3 Day Smoother Atmospheric Density Estimate  $\Delta\rho/\rho$  & Error Covariance Envelope ( $2\sigma$ )

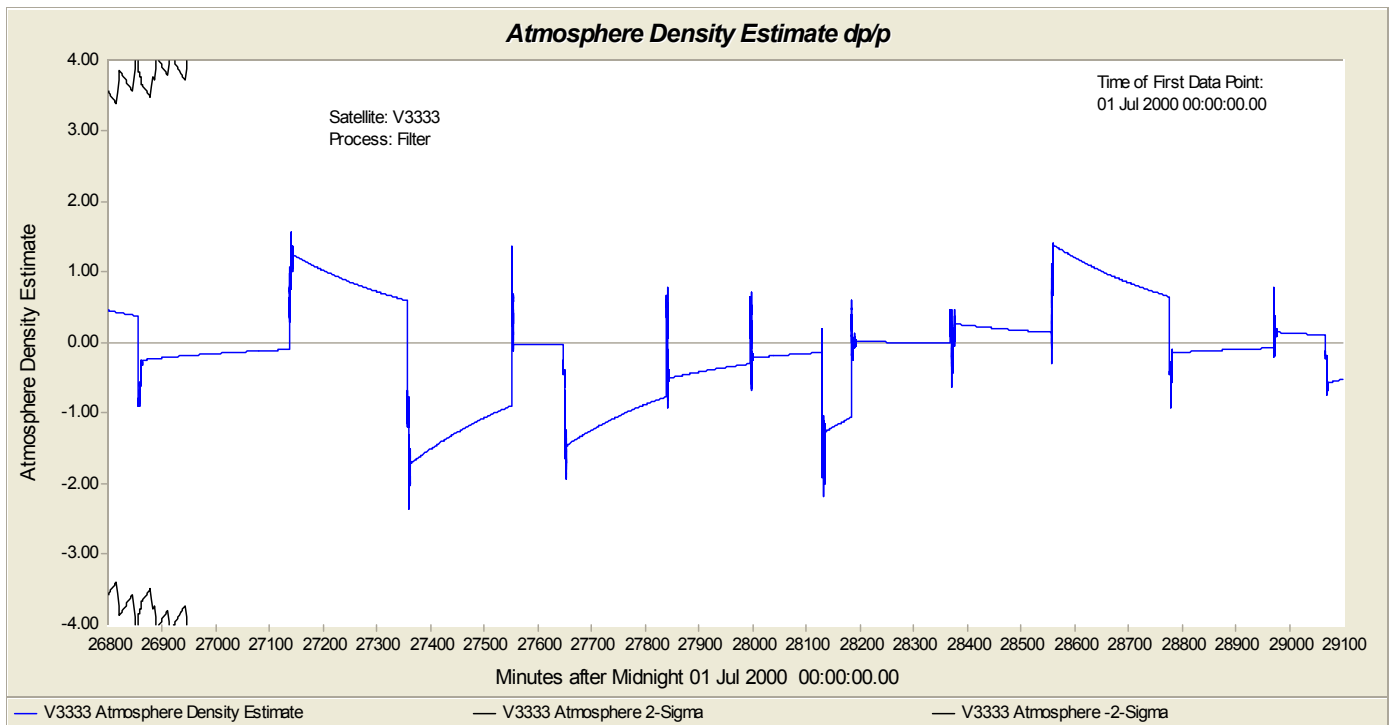


Figure 18: 2 Day Filter Atmospheric Density Estimate  $\Delta\rho/\rho$



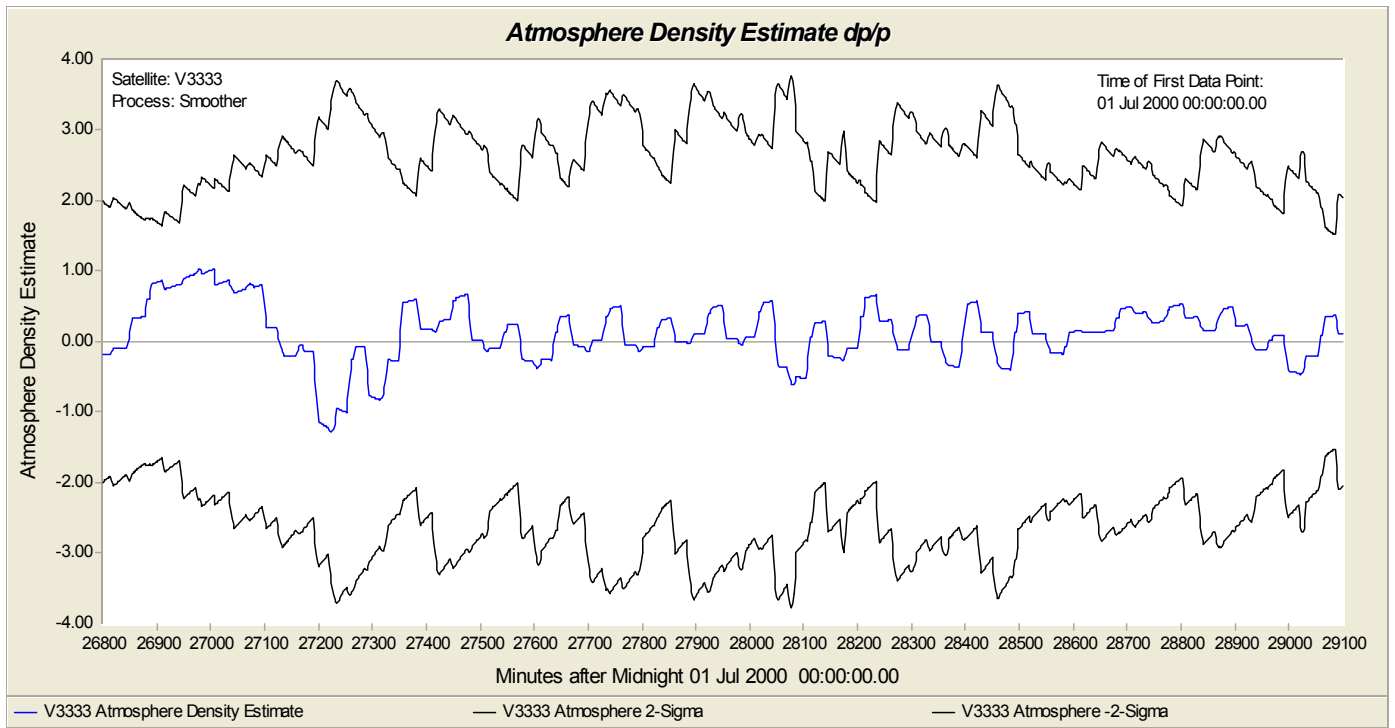


Figure 19: 2 Day Smoother Atmospheric Density Estimate  $\Delta\rho/\rho$

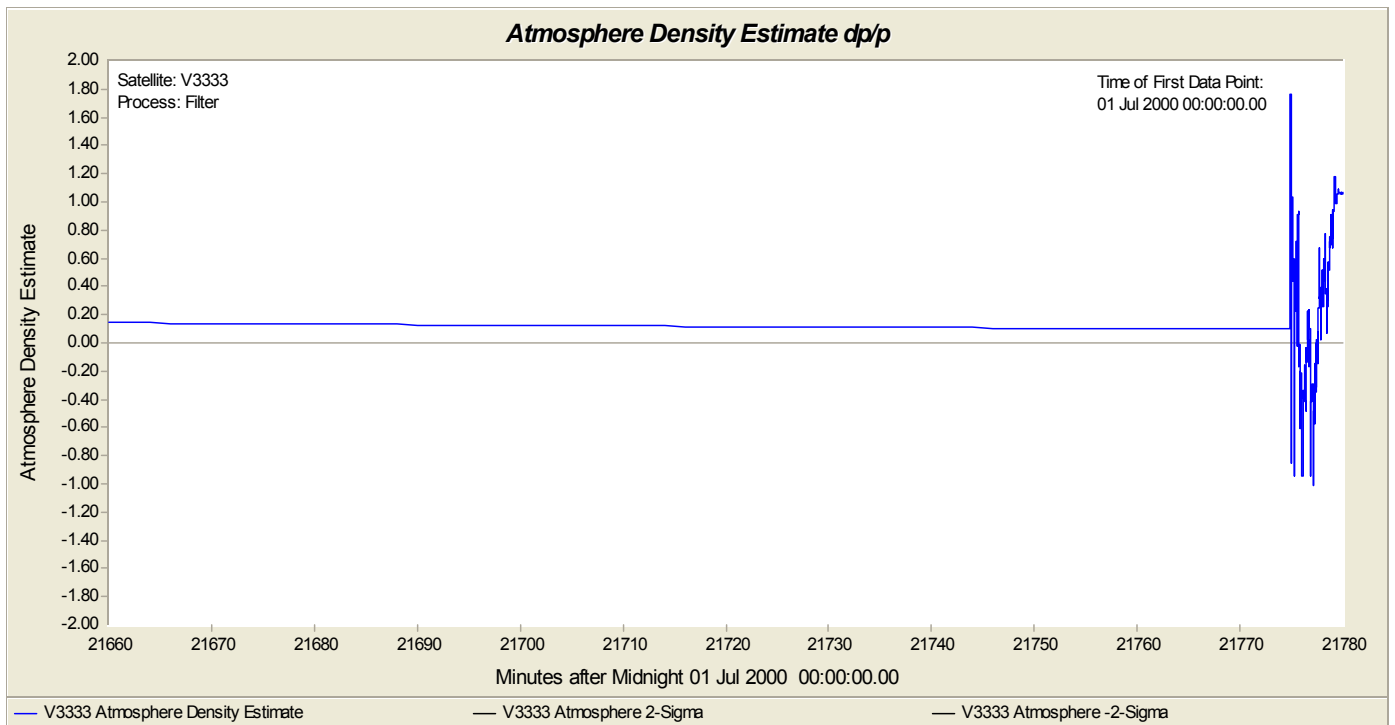


Figure 20: 2 Hour Filter Atmospheric Density Estimate  $\Delta\rho/\rho$

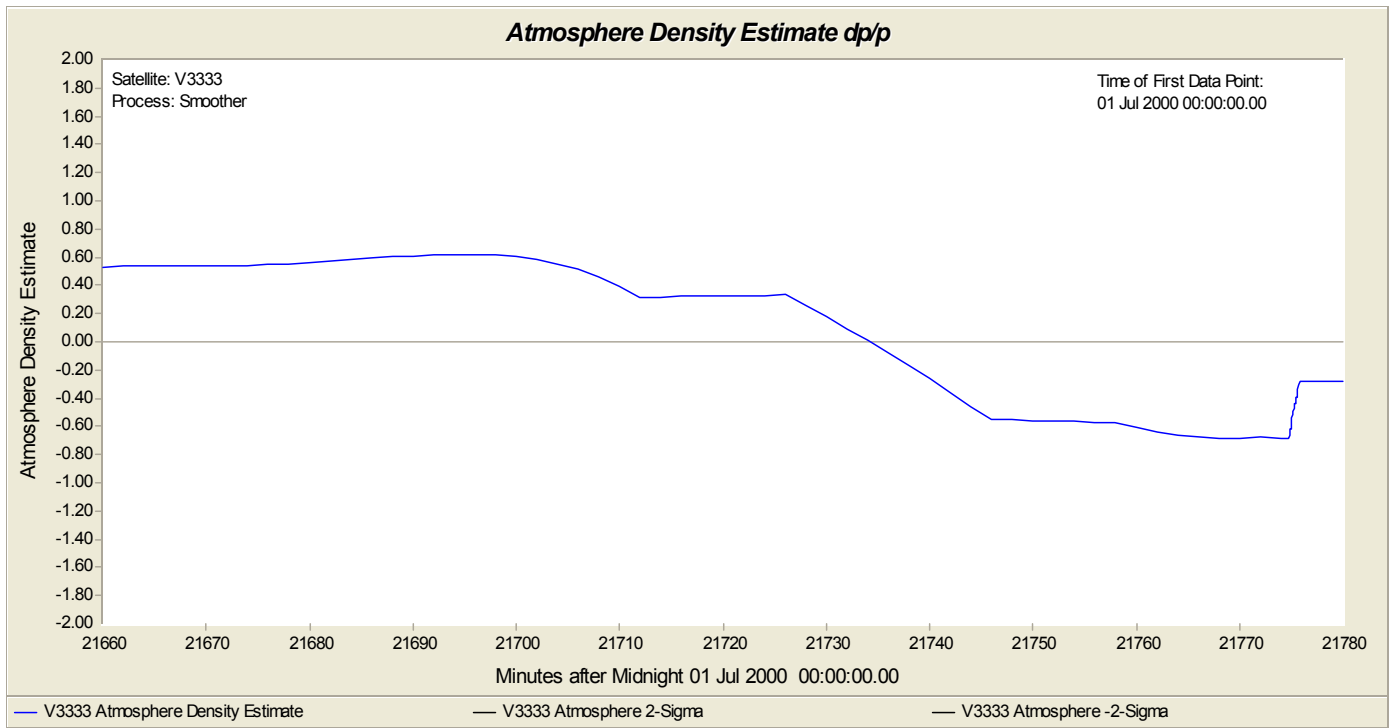


Figure 21: 2 Hour Smoother Atmospheric Density Estimate  $\Delta\rho/\rho$  (Splined  $a_P$ )

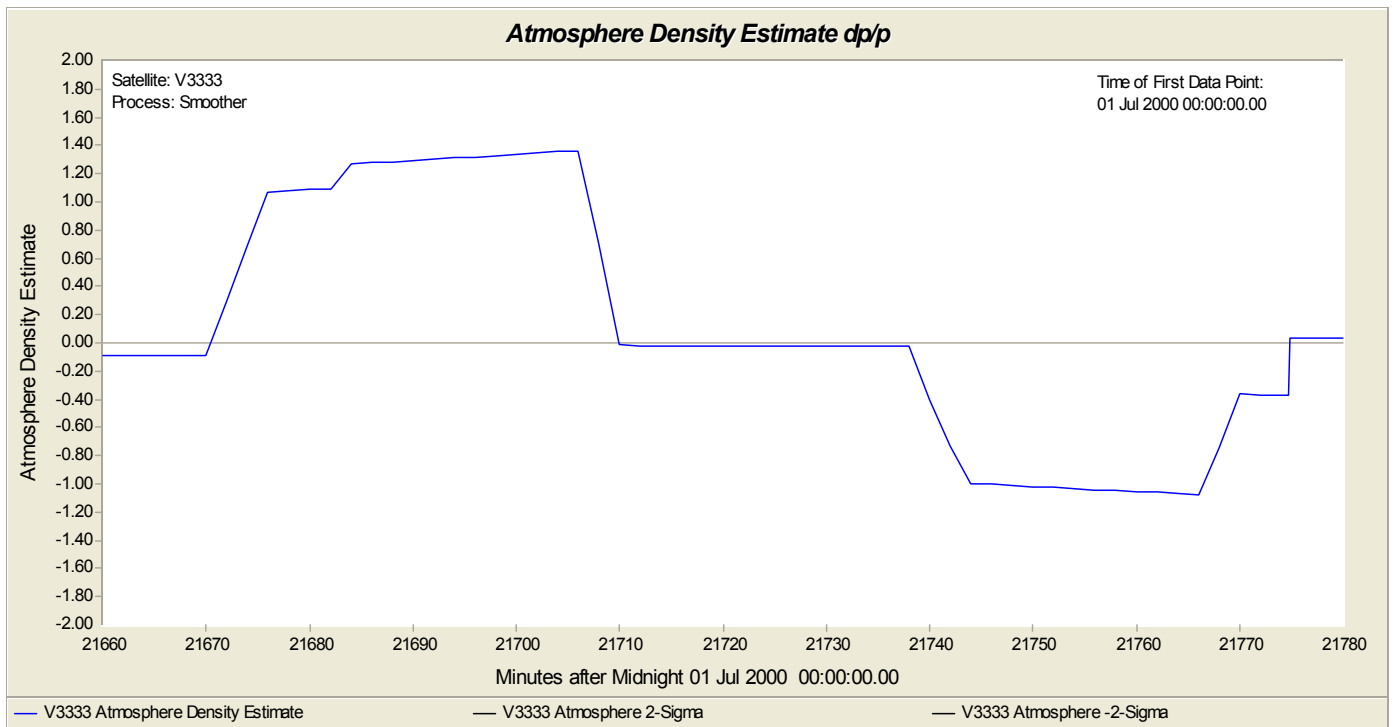


Figure 22: 2 Hour Smoother Atmospheric Density Estimate  $\Delta\rho/\rho$  (Discontinuous  $a_P$ )

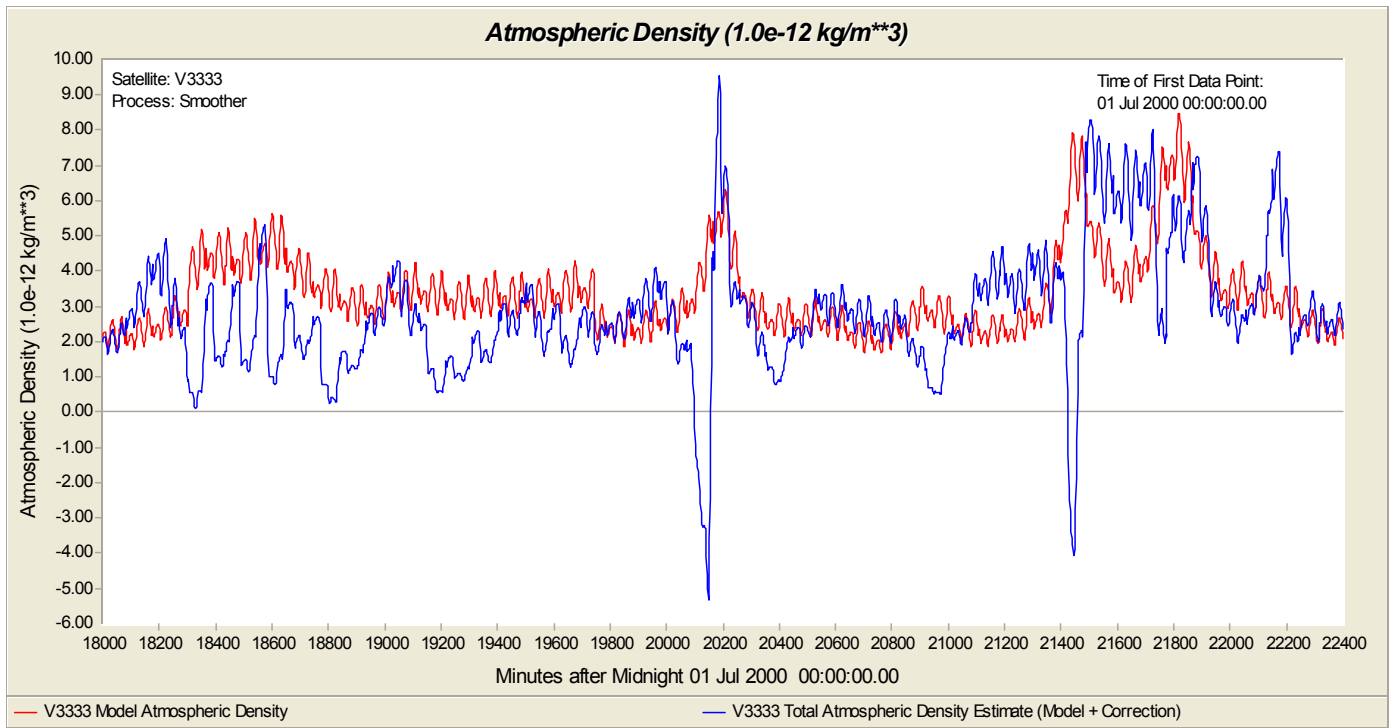


Figure 23: Comparison of Total Atmospheric Density Estimate with Jacchia 1971

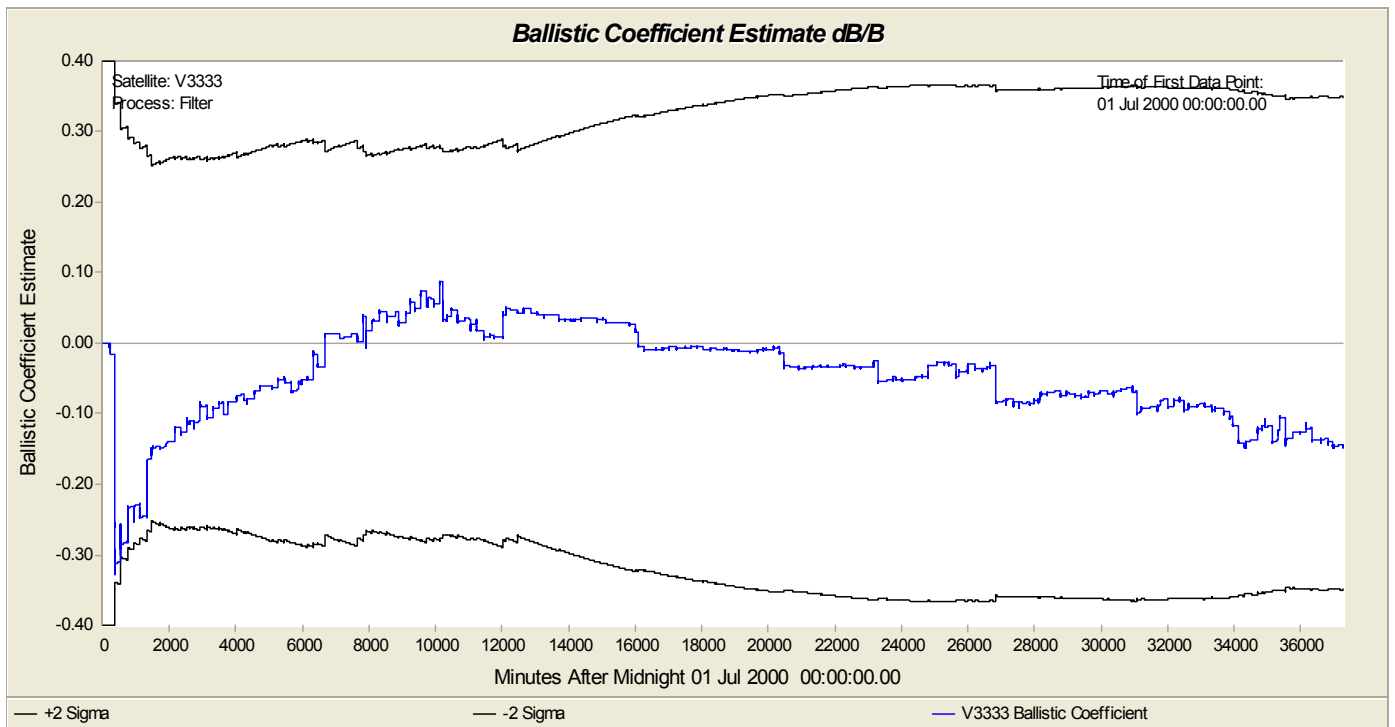


Figure 24: Filter Ballistic Coefficient Estimate & Error Covariance Envelope ( $2\sigma$ )

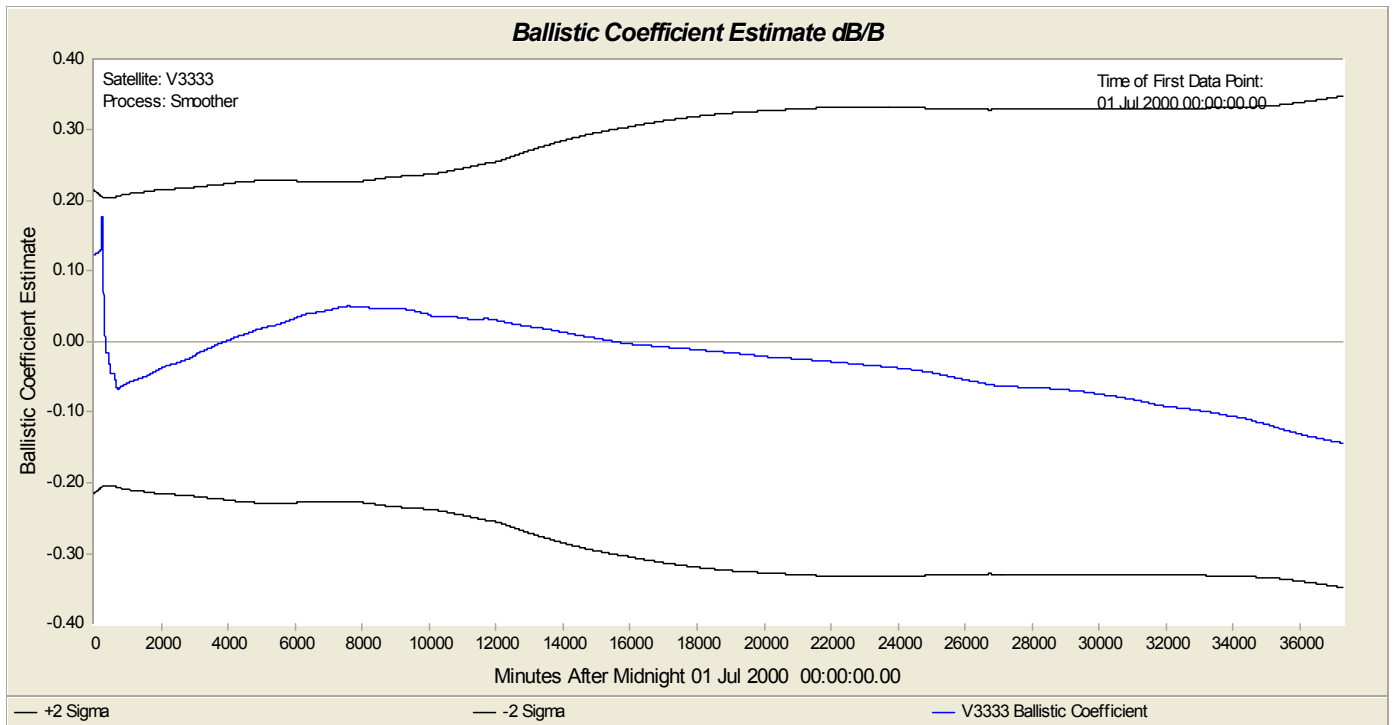


Figure 25: Smoother Ballistic Coefficient Estimate & Error Covariance Envelope ( $2\sigma$ )

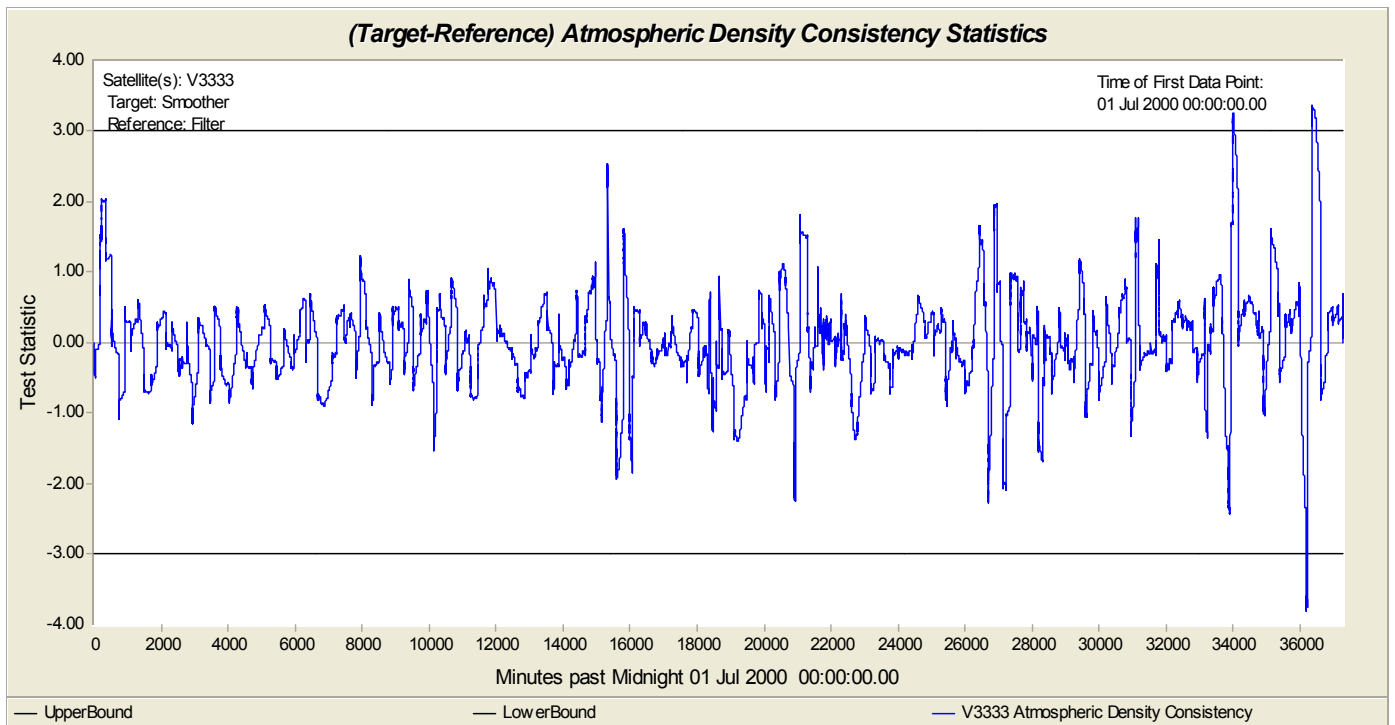


Figure 26: Atmospheric Density Consistency Test Failure with  $a_P$  Discontinuities

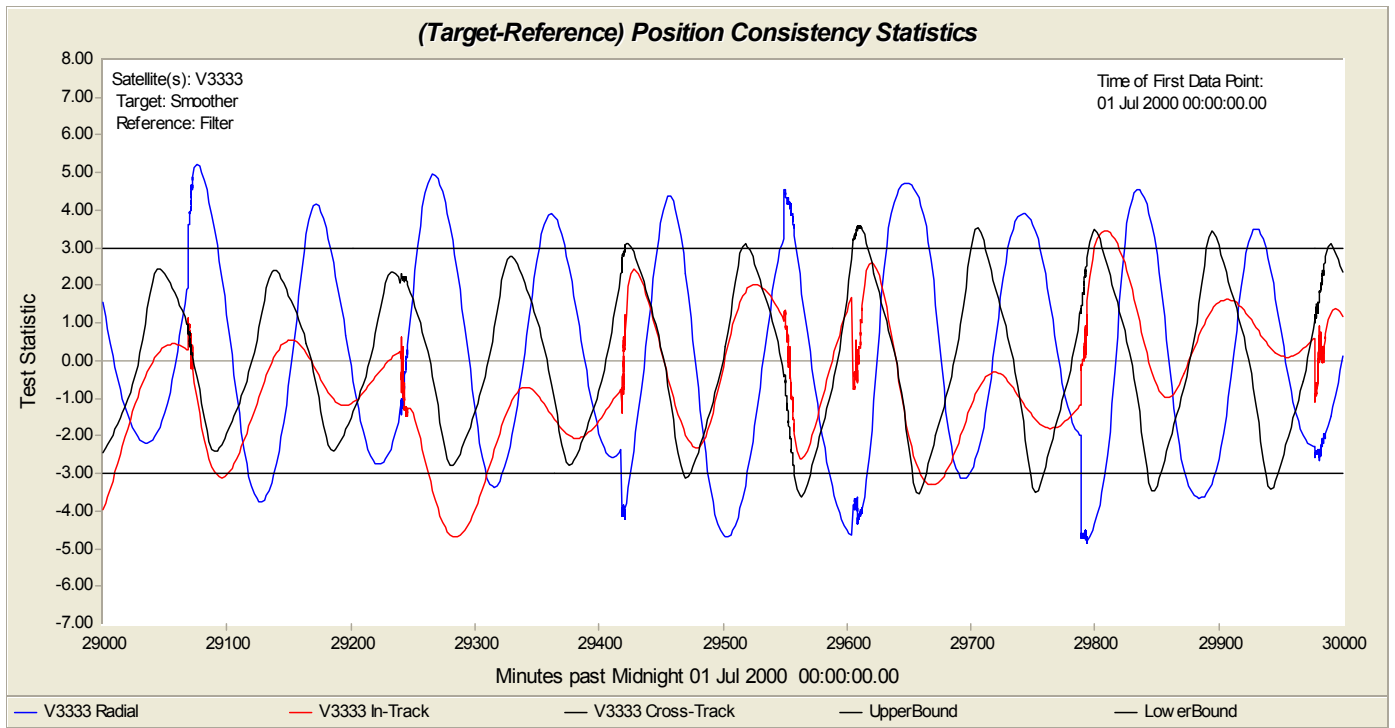


Figure 27: Position Consistency Test Failure with  $a_P$  Discontinuities

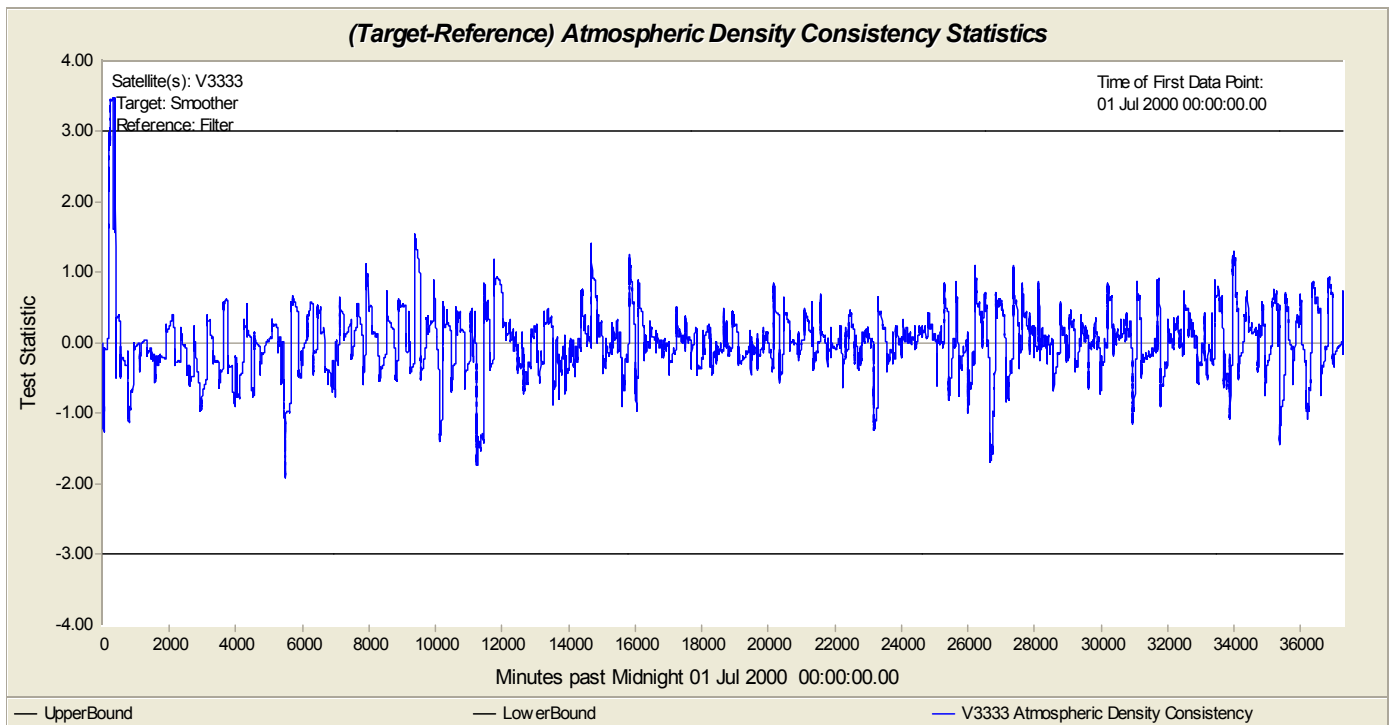


Figure 28: Atmospheric Density Consistency Test Success with  $a_P$  Splines

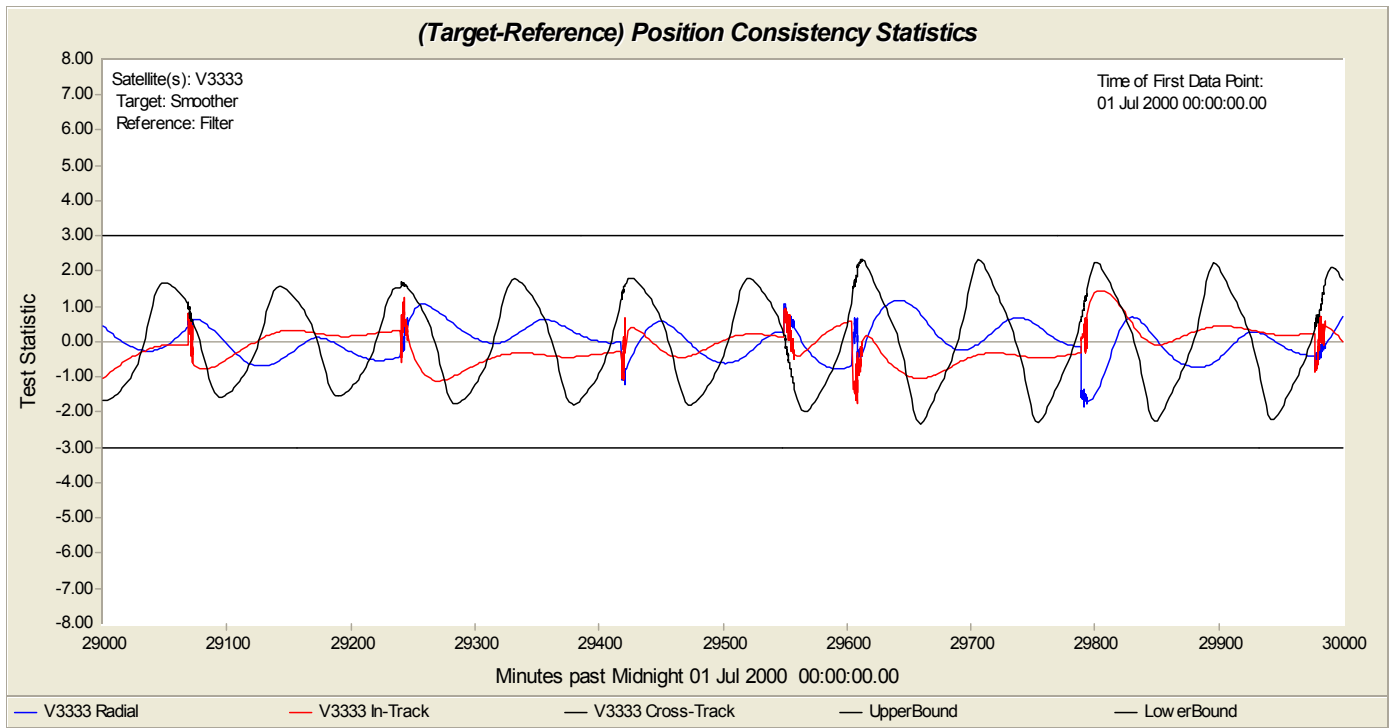


Figure 29: Position Consistency Test Success with  $a_P$  Splines

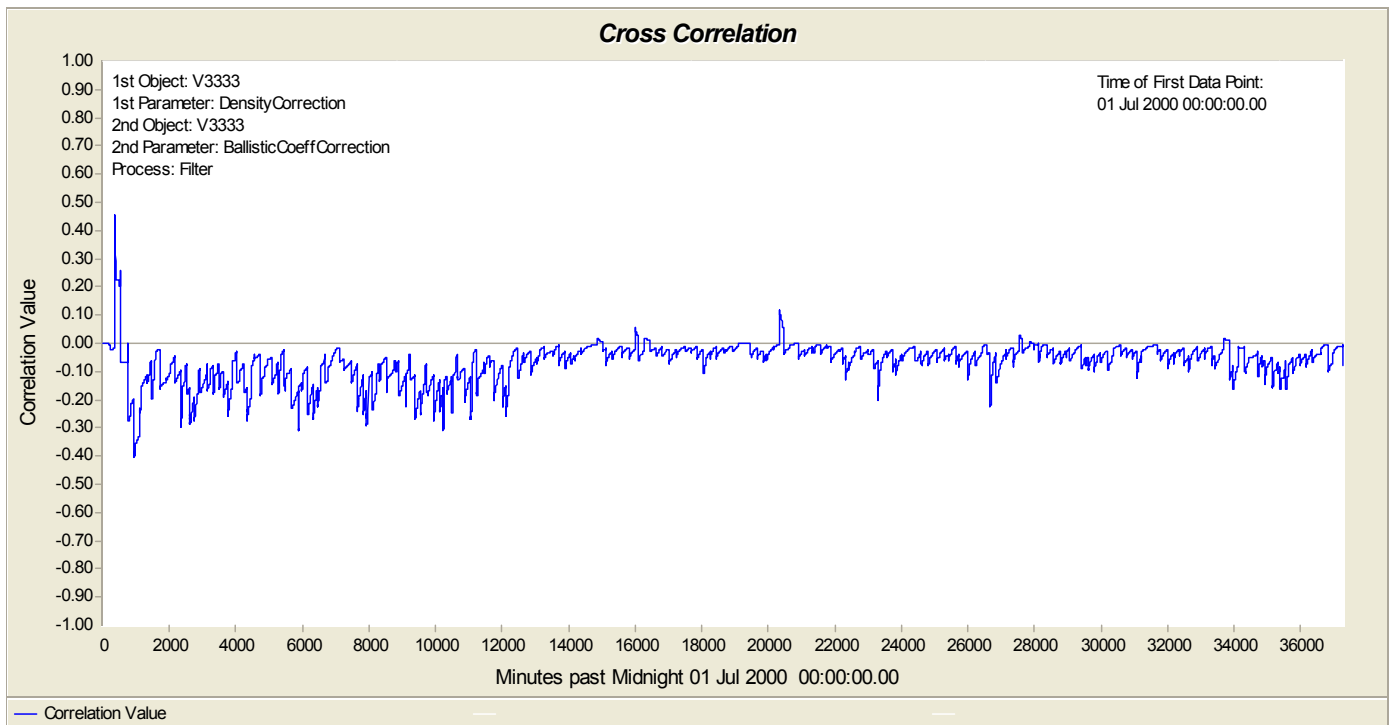


Figure 30: Filter Cross Correlation Atmospheric Density and Ballistic Coefficient

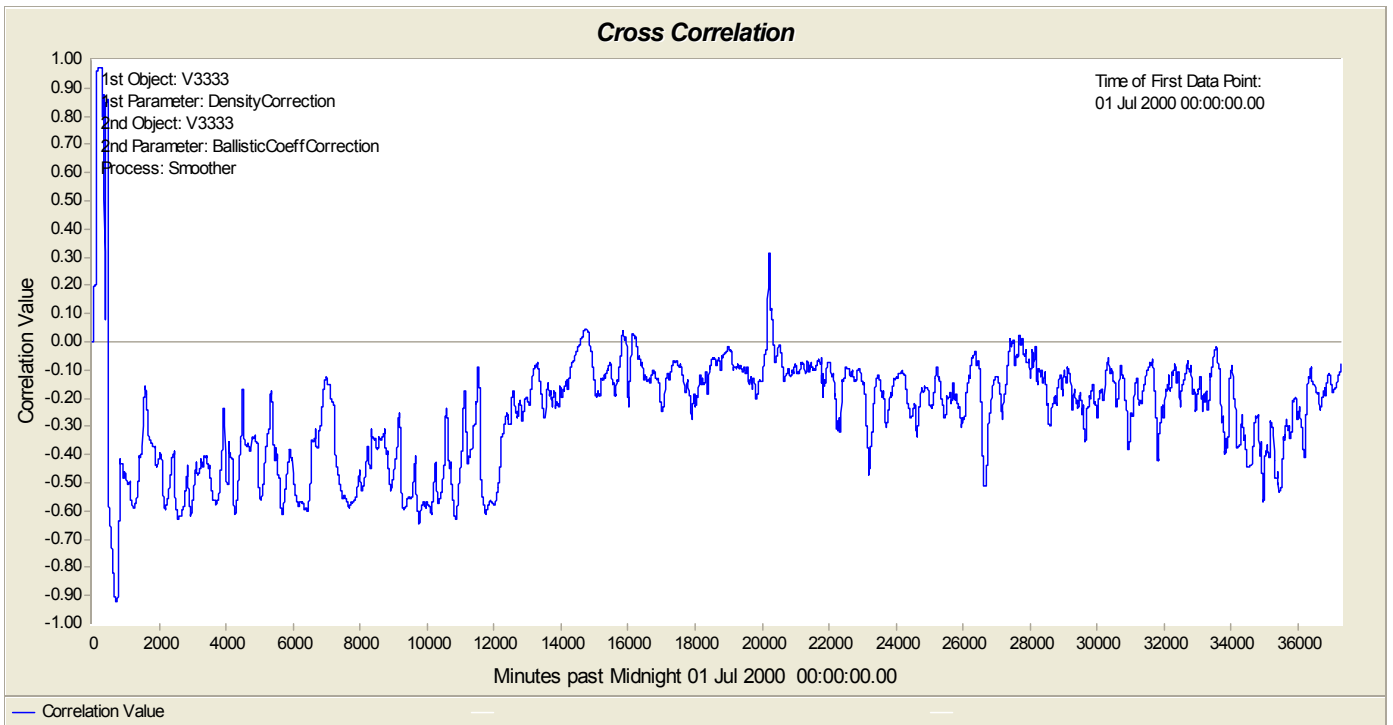


Figure 31: Smoother Cross Correlation Atmospheric Density and Ballistic Coefficient

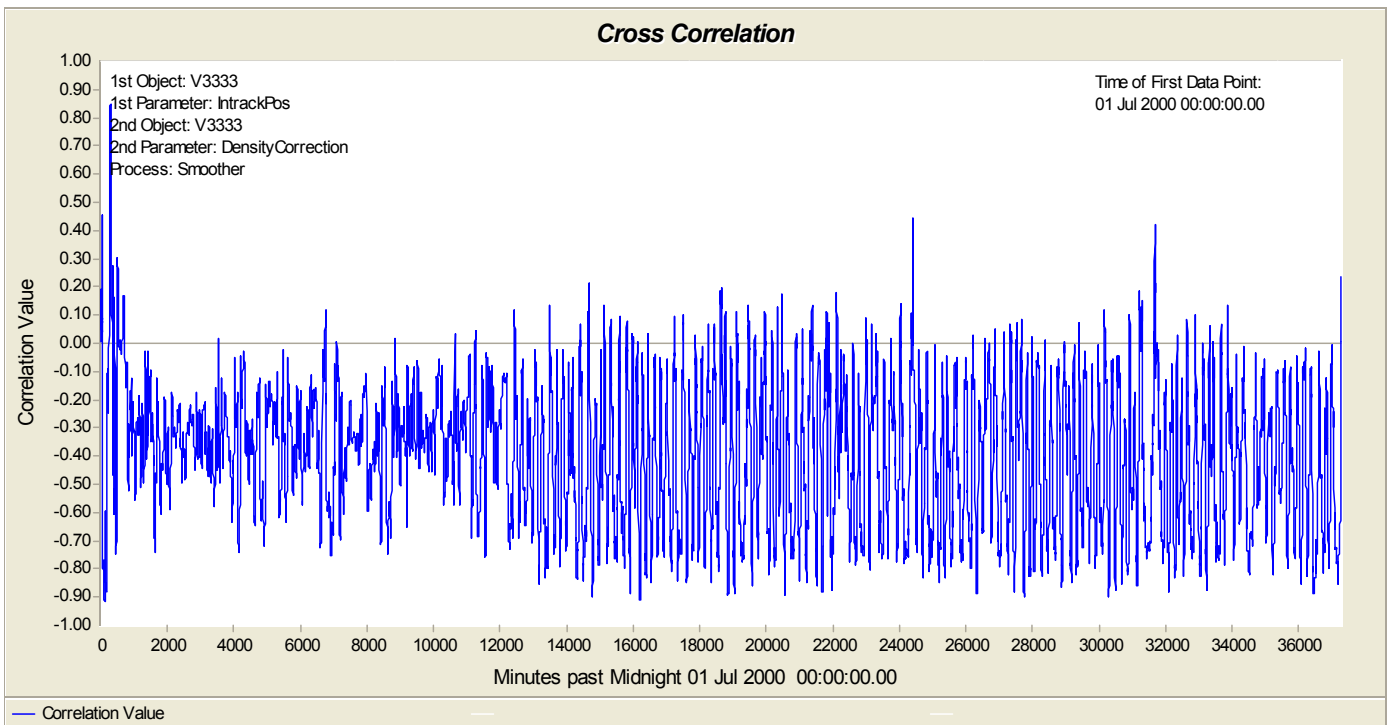


Figure 32: Smoother Cross Correlation Atmospheric Density and Intrack Position

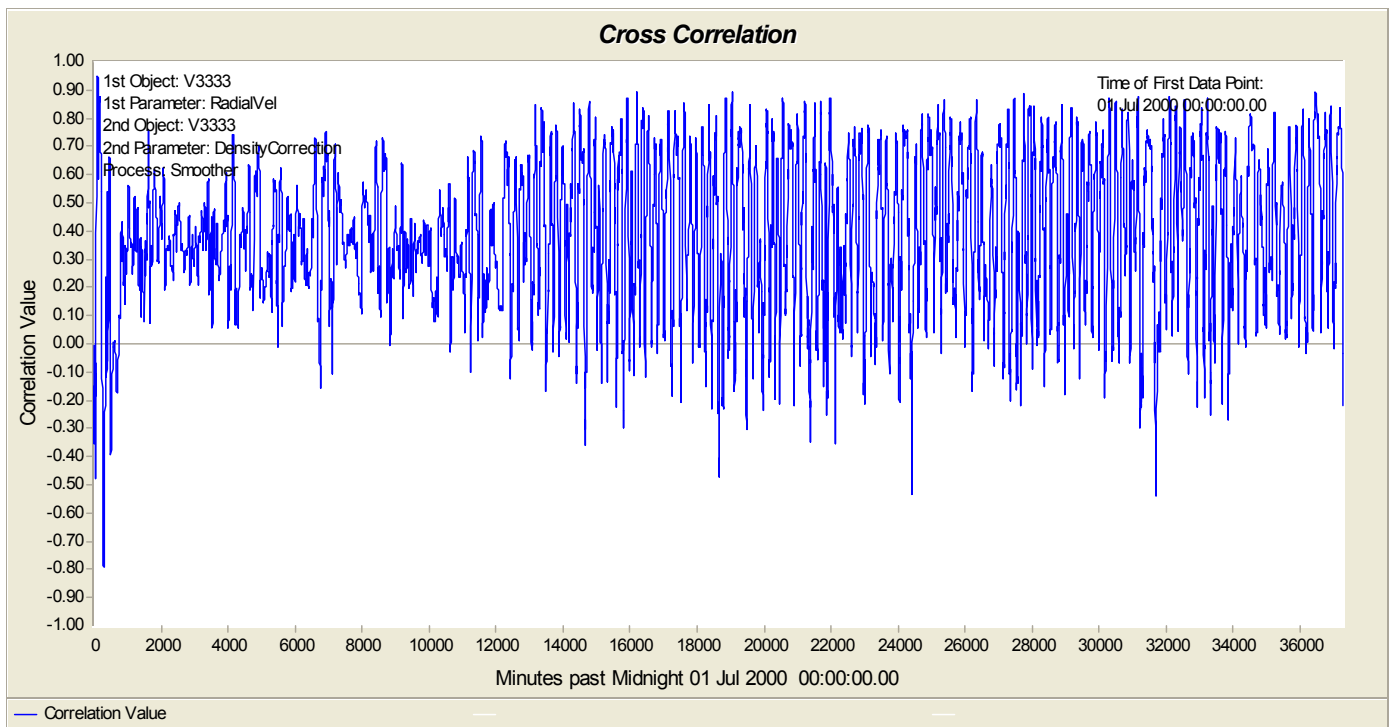


Figure 33: Smoother Cross Correlation Atmospheric Density and Radial Velocity

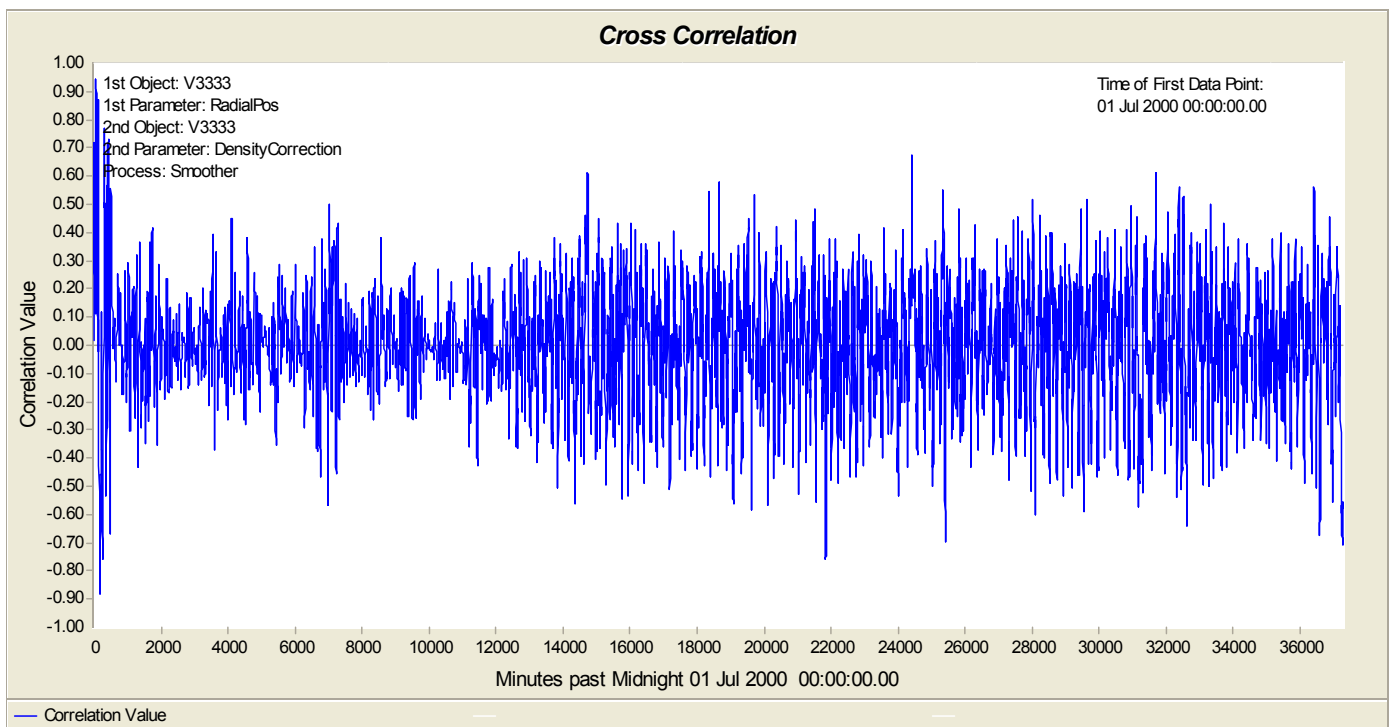


Figure 34: Smoother Cross Correlation Atmospheric Density and Radial Position



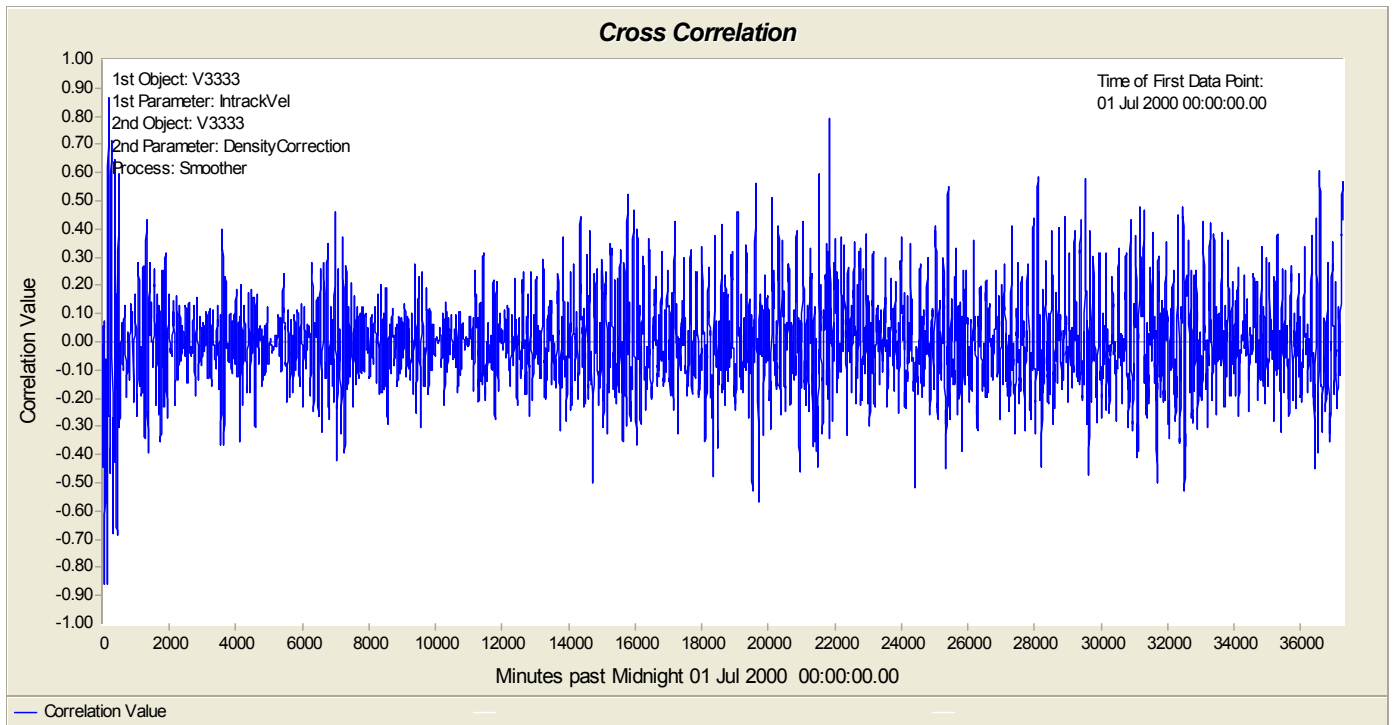


Figure 35: Smoother Cross Correlation Atmospheric Density and Intrack Velocity

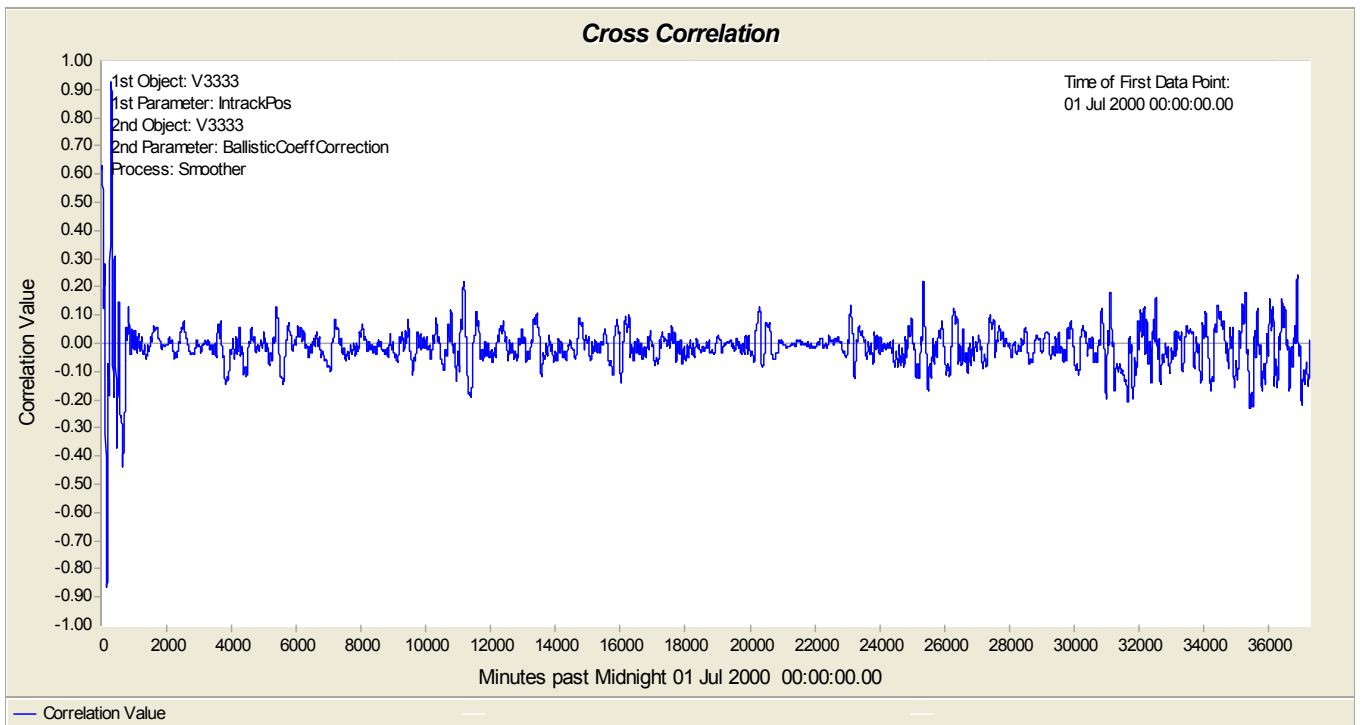


Figure 36: Smoother Cross Correlation Ballistic Coefficient and Intrack Position

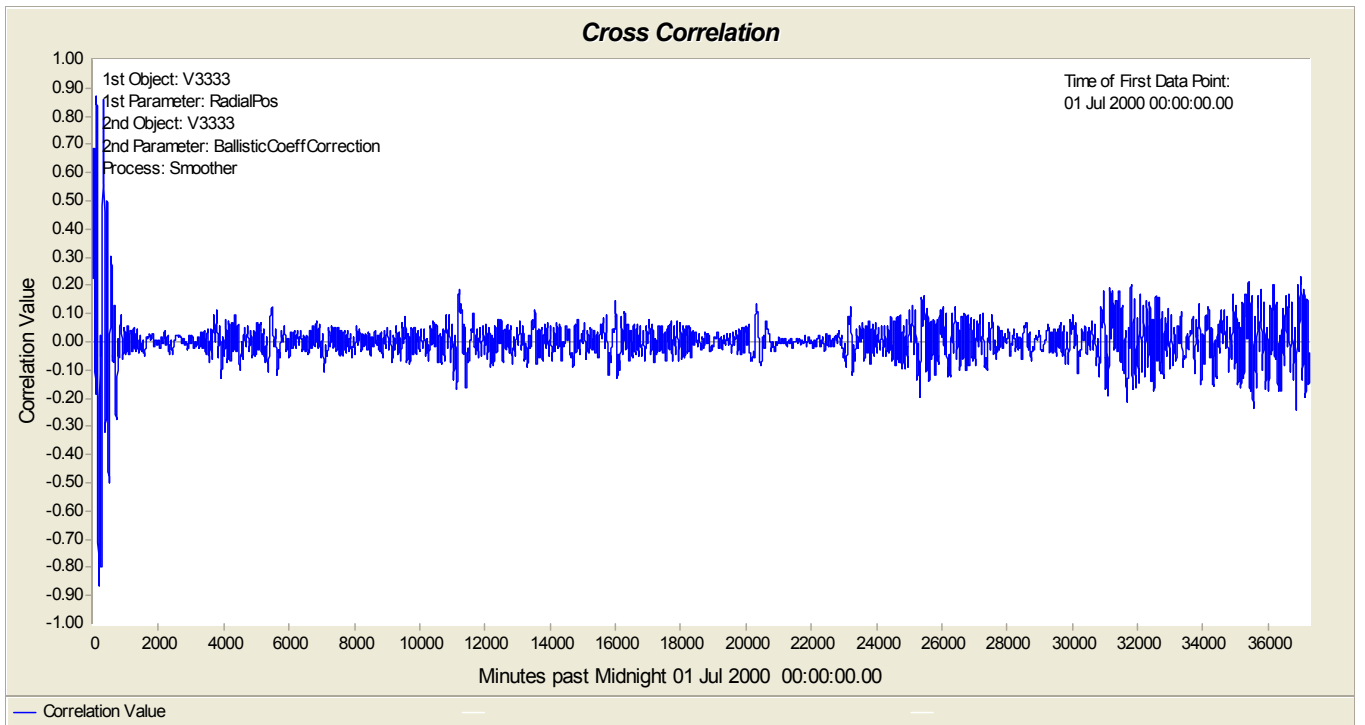


Figure 37: Smoother Cross Correlation Ballistic Coefficient and Radial Position

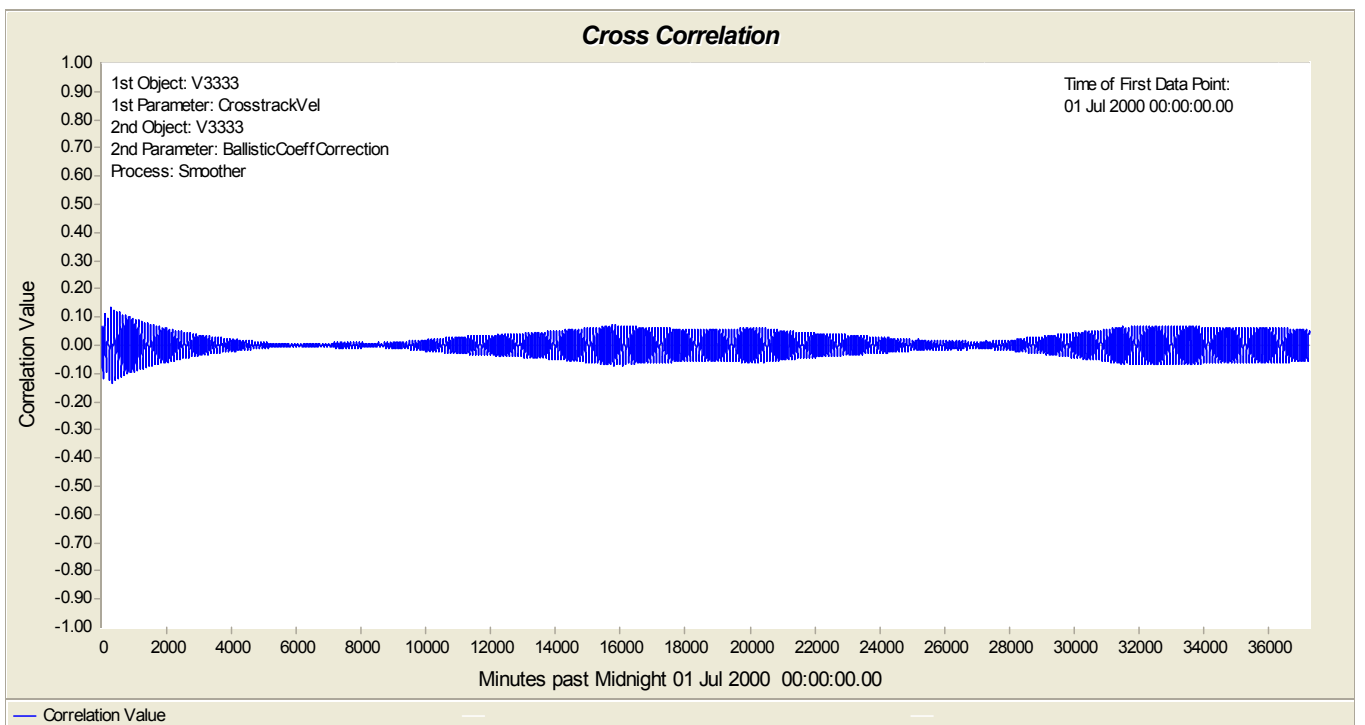


Figure 38: Smoother Cross Correlation Ballistic Coefficient and Crosstrack Velocity

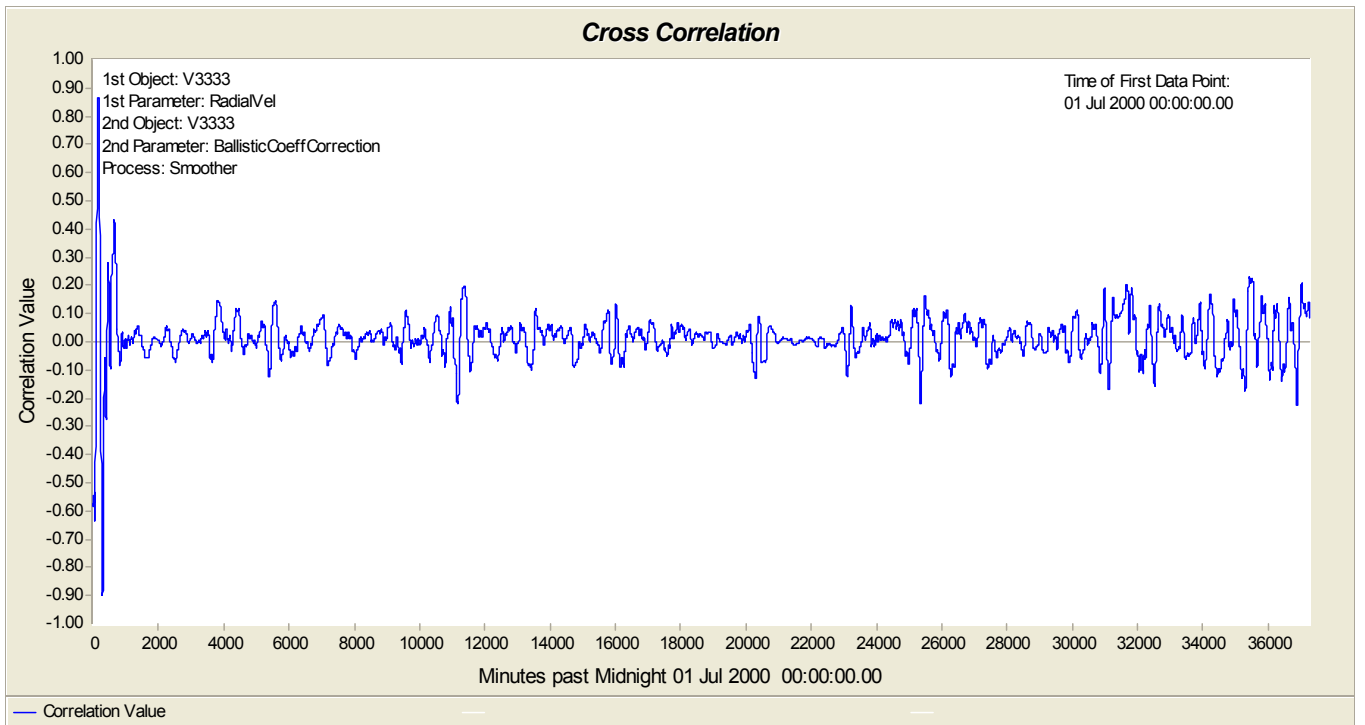


Figure 39: Smoother Cross Correlation Ballistic Coefficient and Radial Velocity

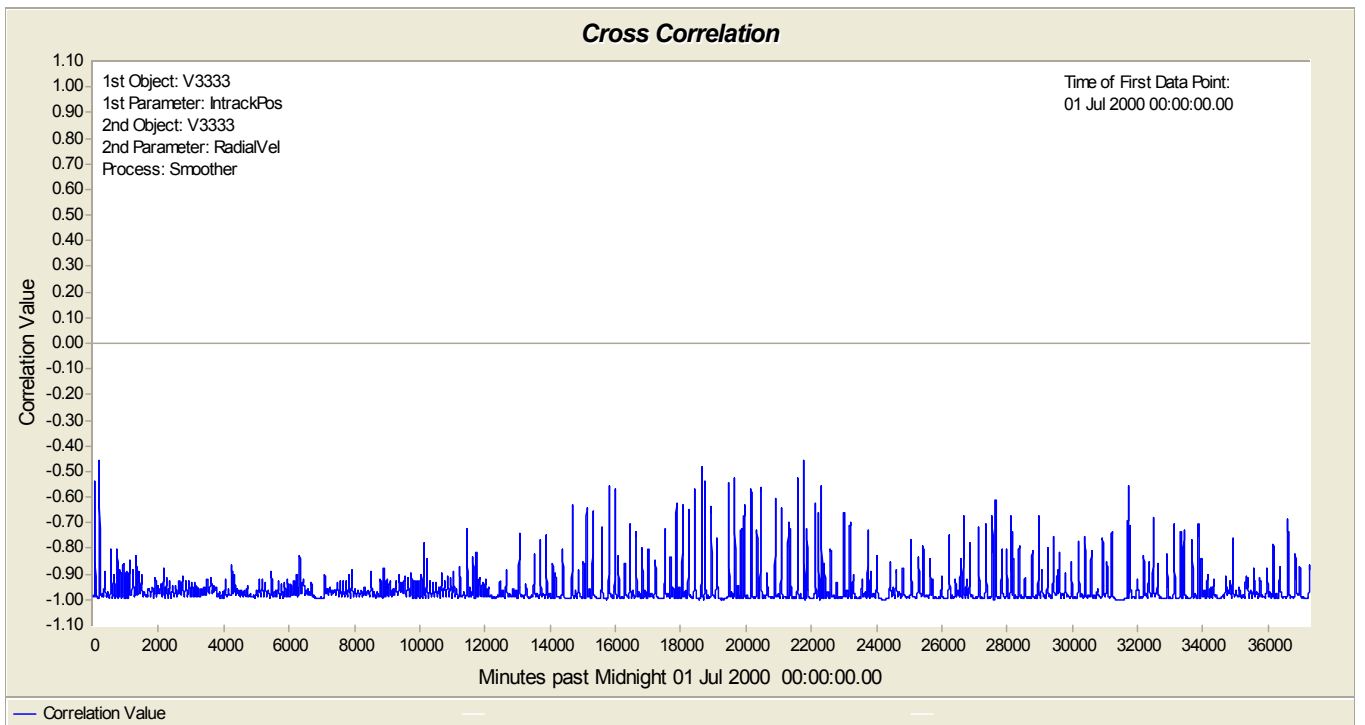


Figure 40: Smoother Cross Correlation Radial Velocity and Intrack Position

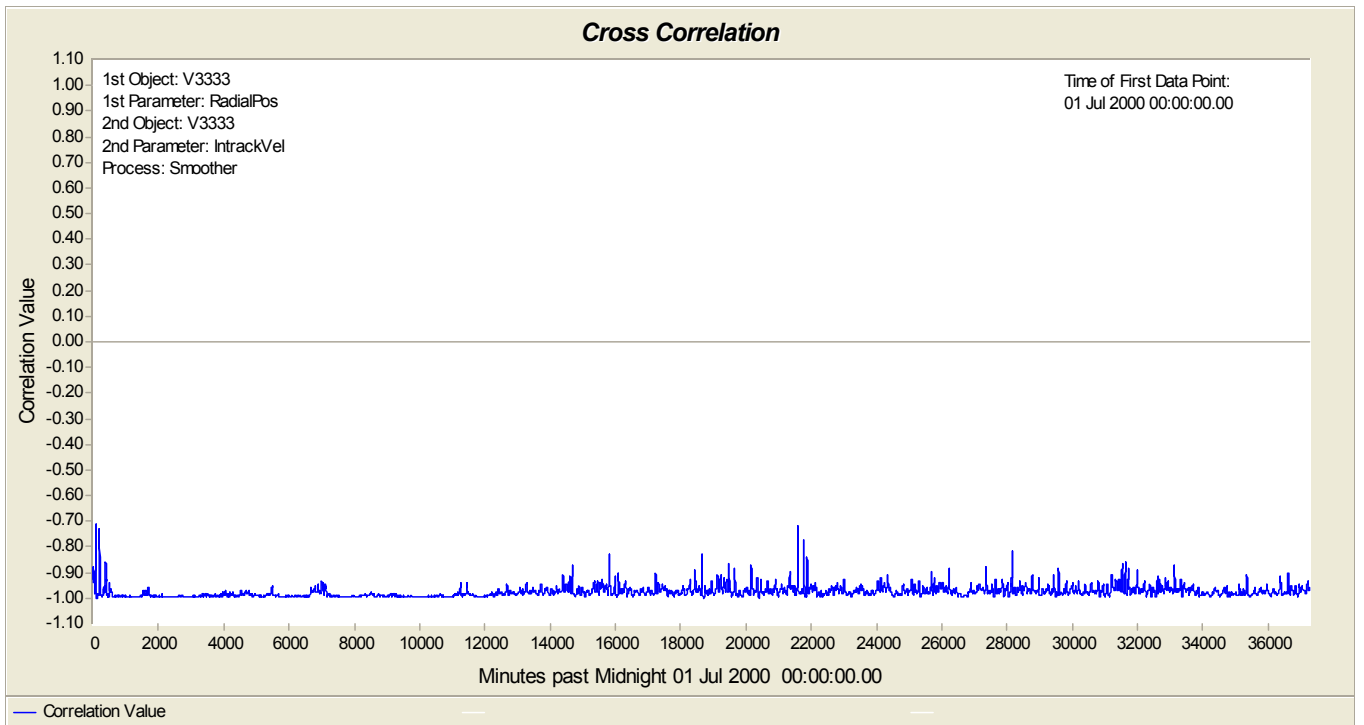


Figure 41: Smoother Cross Correlation Radial Position and Intrack Velocity

### 6.3 $a_P$ Values

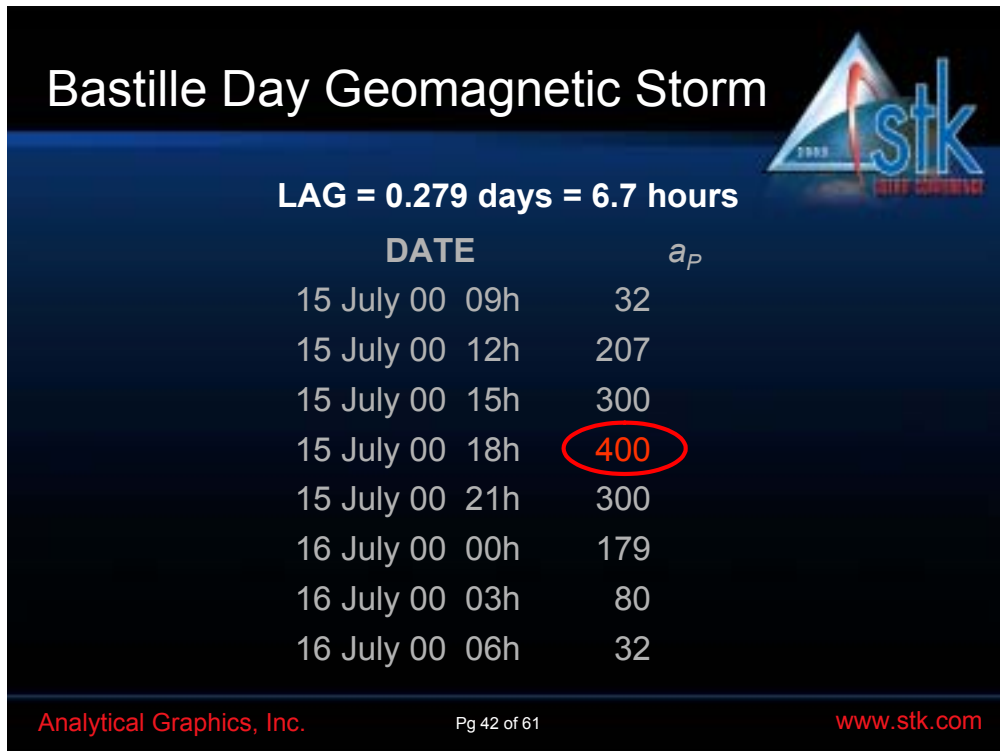


Figure 42:  $a_P$  Values for Bastille Day Geomagnetic Storm

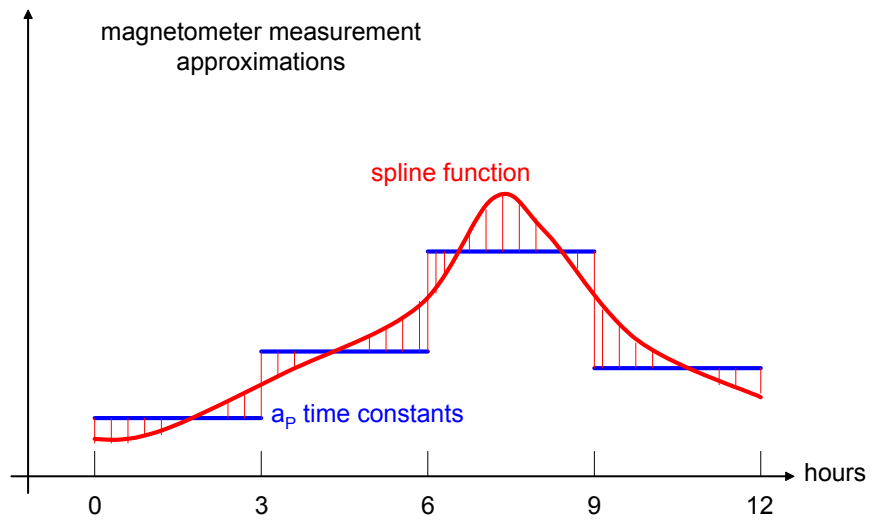


Figure 43:  $a_p$  Spline Cartoon